Drosophila models of pathogenic copy-number variant genes show global and non-neuronal defects during development

Short title: Non-neuronal defects of fly homologs of CNV genes

Tanzeen Yusuff[1,4], Matthew Jensen[1,4], Sneha Yennawar[1,4], Lucilla Pizzo[1], Siddharth Karthikeyan[1], Dagny J. Gould[1], Avik Sarker[1], Erika Gedvilaite[1], Yurika Matsui[1,2], Janani Iyer[1], Zhi-Chun Lai[1,2], and Santhosh Girirajan[1,3]*

1. Department of Biochemistry and Molecular Biology, Pennsylvania State University, University Park, PA 16802
2. Department of Biology, Pennsylvania State University, University Park, PA 16802
3. Department of Anthropology, Pennsylvania State University, University Park, PA 16802

[4] contributed equally to work

*Correspondence:

Santhosh Girirajan, MBBS, PhD

205A Life Sciences Building

Pennsylvania State University

University Park, PA 16802

E-mail: sxg47@psu.edu

Phone: 814-865-0674

ABSTRACT

While rare pathogenic copy-number variants (CNVs) are associated with both neuronal and non-neuronal phenotypes, functional studies evaluating these regions have focused on the molecular basis of neuronal defects. We report a systematic functional analysis of non-neuronal defects for homologs of 59 genes within ten pathogenic CNVs and 20 neurodevelopmental genes in *Drosophila melanogaster*. Using wing-specific knockdown of 136 RNA interference lines, we identified qualitative and quantitative phenotypes in 72/79 homologs, including 21 lines with severe wing defects and six lines with lethality. In fact, we found that 10/31 homologs of CNV genes also showed complete or partial lethality at larval or pupal stages with ubiquitous knockdown. Comparisons between eye and wing-specific knockdown of 37/45 homologs showed both neuronal and non-neuronal defects, but with no correlation in the severity of defects. We further observed disruptions in cell proliferation and apoptosis in larval wing discs for 23/27 homologs, and altered Wnt, Hedgehog and Notch signaling for 9/14 homologs, including *AATF/Aatf*, *PPP4C/Pp4-19C*, and *KIF11/Klp61F*. These findings were further supported by tissue-specific differences in expression patterns of human CNV genes, as well as connectivity of CNV genes to signaling pathway genes in brain, heart and kidney-specific networks. Our findings suggest that multiple genes within each CNV differentially affect both global and tissue-specific developmental processes within conserved pathways, and that their roles are not restricted to neuronal functions.

AUTHOR SUMMARY

Rare copy-number variants (CNVs), or large deletions and duplications in the genome, are associated with both neuronal and non-neuronal clinical features. Previous functional studies for these disorders have primarily focused on understanding the cellular mechanisms for neurological and behavioral phenotypes. To understand how genes within these CNVs contribute to developmental defects in non-neuronal tissues, we assessed 79 homologs of CNV and known neurodevelopmental genes in *Drosophila* models. We found that most homologs showed developmental defects when knocked down in the adult fly wing, ranging from mild size changes to severe wrinkled wings or lethality. Although a majority of homologs tested showed defects when knocked down specifically in wings and eyes, we found no correlation in the severity of the observed defects in these two tissues. A subset of the homologs showed disruptions in cellular processes in the developing fly wing, including alterations in cell proliferation, apoptosis, and cellular signaling pathways. Furthermore, human CNV genes also showed differences in gene expression patterns and interactions with signaling pathway genes across multiple human tissues. Our findings suggest that genes within CNV disorders affect global developmental processes in both neuronal and non-neuronal tissues.

INTRODUCTION

Rare copy-number variants (CNV), or deletions and duplications in the genome, are associated with neurodevelopmental disorders such as autism, intellectual disability (ID), and schizophrenia [1,2]. While dosage alteration of CNV regions contribute predominantly to defects in nervous system development, several CNV-associated disorders also lead to early developmental features involving other organ systems [3,4], including cardiac defects [5,6], kidney malformations [7], craniofacial features [3], and skeletal abnormalities [8]. In fact, an overall survey of ten rare disease-associated CNVs among individuals within the DECIPHER database [9] showed a wide range of non-neuronal phenotypes across multiple organ systems for each CNV disorder (**S1 Fig., S1 Data**). For example, the 1q21.1 deletion causes variable expression of multiple neuronal and non-neuronal phenotypes, including developmental delay, autism, and schizophrenia as well as craniofacial features, cataracts, cardiac defects, and skeletal abnormalities [10–12]. Additionally, while the 7q11.23 deletion associated with Williams-Beuren syndrome (WBS) causes neuropsychiatric and behavioral features, other non-neuronal phenotypes, including supravalvular aortic stenosis, auditory defects, hypertension, diabetes mellitus, and musculoskeletal and connective tissue anomalies, are also observed among the deletion carriers [13].

Despite the prevalence of non-neuronal phenotypes among CNV carriers, functional studies of CNV genes have primarily focused on detailed assessments of neuronal and behavioral phenotypes in model systems. For example, mouse models for the 16p11.2 deletion exhibited post-natal lethality, reduced brain size and neural progenitor cell count, motor and habituation defects, synaptic defects, and behavioral defects [14–16]. Similarly, mouse models for the 3q29 deletion showed decreased weight and brain size, increased locomotor activity, increased startle

80 response, and decreased spatial learning and memory [17,18]. However, fewer studies have
81 focused on detailed evaluation of non-neuronal phenotypes in functional models of CNV
82 disorders. For example, Arbogast and colleagues evaluated obesity and metabolic changes in
83 16p11.2 deletion mice, which showed reduced weight and impaired adipogenesis [19]. While
84 Haller and colleagues showed that mice with knockdown of *MAZ,* a gene within the 16p11.2
85 deletion region, exhibit genitourinary defects observed in individuals with the deletion [20],
86 mouse studies for other homologs of 16p11.2 genes, including *TAOK2*, *KCTD13*, and *MAPK3,*
87 have only focused on assessing neuronal defects [21–25]. Furthermore, Dickinson and
88 colleagues reported a high-throughput analysis of essential genes in mice and identified both
89 neuronal and non-neuronal phenotypes for individual gene knockouts, including more than 400
90 genes that lead to lethality [26]. While these efforts aided in implicating novel genes with human
91 disease, our understanding of how genes associated with neurodevelopmental disorders
92 contribute towards non-neuronal phenotypes is still limited. Therefore, a large-scale analysis of
93 non-neuronal phenotypes is necessary to identify specific candidate genes within CNV regions
94 and associated biological mechanisms that contribute towards these phenotypes.
95 *Drosophila melanogaster* is an excellent model system to evaluate homologs of
96 neurodevelopmental genes, as many developmental processes and signaling pathways are
97 conserved between humans and flies [27]. In fact, over 75% of human disease genes have
98 homologs in *Drosophila*, including many genes involved in cellular signaling processes [28,29].
99 We recently examined the contributions of individual *Drosophila* homologs of 28 genes within
100 the 16p11.2 and 3q29 deletion regions towards specific neurodevelopmental phenotypes,
101 including rough eye phenotypes and defects in climbing ability, axon targeting, neuromuscular
102 junction, and dendritic arborization [30,31]. While these findings implicated multiple genes

103 within each CNV region towards conserved cellular processes in neuronal tissues, the conserved
104 role of these genes in non-neuronal tissues is not well understood. The *Drosophila* wing is an
105 effective model system to evaluate such developmental defects, as key components of conserved
106 signaling pathways, such as Notch, epidermal growth factor receptor (EGFR), Hegdehog, and
107 Wnt pathways, were identified using fly wing models [32–38]. Although fly wing phenotypes
108 cannot be directly translated to human phenotypes, defects observed in fly wings can be used to
109 assess how homologs of human disease genes alter conserved cellular and developmental
110 mechanisms. For example, Wu and colleagues showed that overexpression of the *Drosophila*
111 homolog for *UBE3A*, associated with Angelman syndrome, leads to abnormal wing and eye
112 morphology defects [39]. Furthermore, *Drosophila* mutant screens for developmental
113 phenotypes, including wing defects, were used to identify conserved genes for several human
114 genetic diseases, including Charcot-Marie-Tooth disease and syndromic microcephaly [40].
115 Kochinke and colleagues also recently performed a large-scale screening of ID-associated genes,
116 and found an enrichment of wing trichome density and missing vein phenotypes in ID genes
117 compared to control gene sets [41]. Hence, the fly wing provides a model system that is ideal for
118 evaluating the contributions of individual homologs of CNV genes towards cellular and
119 developmental defects.

120 In this study, we tested tissue-specific and cellular phenotypes of 79 total fly homologs,
121 including 59 fly homologs of human genes within ten pathogenic CNV regions and 20 genes
122 associated with neurodevelopmental disorders. We used the adult fly wing to evaluate
123 phenotypes in a non-neuronal tissue, and observed a wide range of robust qualitative and
124 quantitative wing phenotypes among 136 RNA interference (RNAi) lines, including size defects,
125 ectopic and missing veins, severe wrinkling, and lethality. Further analysis of cellular

126 phenotypes revealed disruptions in conserved developmental processes in the larval imaginal
127 wing disc, including altered levels of cell proliferation and apoptosis as well as altered
128 expression patterns in the Wnt, Hedgehog, and Notch signaling pathways. However, we found
129 no correlation in the severity of phenotypes observed with wing and eye-specific knockdown.
130 These findings were further supported by differences in expression patterns and network
131 connectivity of human CNV genes across different tissues. Our analysis emphasizes the
132 importance of multiple genes within each CNV region towards both global and tissue-specific
133 developmental processes.

134 **RESULTS**

135 **Knockdown of fly homologs of CNV genes contribute to a range of wing defects**

136 We used the *bx*^{MS1096}*-GAL4* wing-specific driver to assess a total of 136 RNAi lines for 59 fly
137 homologs of 130 total human genes within pathogenic CNV regions (chromosomal locations
138 1q21.1, 3q29, 7q11.23, 15q11.2, 15q13.3, 16p11.2, distal 16p11.2, 16p12.1, 16p13.11, and
139 17q12), as well as 20 fly homologs of human genes associated with neurodevelopmental
140 disorders (**S2 Data**). Fly homologs of these genes were identified using the DIOPT orthology
141 prediction tool [42]. We list both the human gene name and the fly gene name for each tested
142 gene as *HUMAN GENE/Fly gene* (i.e. *KCTD13/CG10465*), as well as the human CNV region for
143 context at first instance. We scored 20-25 adult wings for five distinct wing phenotypes in each
144 non-lethal RNAi line, including wrinkled wing, discoloration, ectopic veins, missing veins, and
145 bristle planar polarity phenotypes (**Fig. 1; S3 Data**). We categorized adult female wing
146 phenotypes based on their severity, and performed k-means clustering analysis to categorize each
147 RNAi line by their overall phenotypic severity (**Fig. 2A-B**). We observed four clusters of RNAi
148 lines: 75 lines with no observable qualitative phenotypes (55.2%), 24 lines with mild phenotypes
149 (17.6%), 10 lines with moderate phenotypes (7.4%), 21 lines with severe phenotypes (15.4%),
150 and 6 lines with lethal phenotypes (4.4%), including *ACACA/ACC* within 17q12, *DLG1/dlg1*
151 within 3q29, and *STX1A/Syx1A* within 7q11.23 (**Fig. 2; S3 Data**). We observed severe wrinkled
152 wing phenotypes for 13/79 fly homologs, including *PPP4C/Pp4-19C* within 16p11.2,
153 *ATXN2L/Atx2* within distal 16p11.2, *AATF/Aatf* within 17q12, and *MFI2/Tsf2* within 3q29 (**Fig.**
154 **3A-B, S4 Data**). Interestingly, seven out of ten CNV regions contained at least one homolog that
155 showed lethality or severe wing phenotypes, and five CNV regions (3q29, 16p11.2, distal
156 16p11.2, 16p12.1, and 17q12) had multiple homologs showing lethality or severe wing

157 phenotypes (**Fig. 3A, S4 Data**). For example, RNAi lines for both *UQCRC2/UQCR-C2* and
158 *POLR3E/Sin* within 16p12.1 showed lethality. Within the 3q29 region, *NCBP2/Cbp20* and
159 *MFI2/Tsf2* showed severe phenotypes while *DLG1/dlg1* showed lethality. In contrast, 12/20
160 known neurodevelopmental genes showed no observable wing phenotypes, suggesting that these
161 genes could be responsible for neuronal-specific phenotypes (**Fig. 3B, S4 Data**). We note that
162 18/79 fly homologs showed discordant phenotypes between two or more RNAi lines for the
163 same gene, which could be due to differences in expression of the RNAi construct among these
164 lines (**S4 Data**).

165 Certain qualitative phenotypes were present at a higher frequency in males compared to
166 females among all non-lethal and non-severe RNAi lines (independent of k-means clustering
167 analysis). For example, discoloration (87 lines in males compared to 55 lines in females;
168 $p=1.315\times10^{-4}$, two-tailed Fisher's exact test) and missing vein phenotypes (92 lines in males
169 compared to 29 lines in females; $p=2.848\times10^{-16}$, two-tailed Fisher's exact test) were more
170 commonly observed in males than females (**S3 Data**). In particular, 25/92 lines in males
171 (compared to 1/29 in females) showed a total loss of the anterior crossvein (ACV) (**S3 Data**).
172 We further identified 17 RNAi lines that were lethal in males with wing-specific knockdown of
173 fly homologs. While higher frequencies of wing phenotypes in males could be due to a sex-
174 specific bias of developmental phenotypes, the increased severity we observed in males is most
175 likely due to a stronger RNAi knockdown caused by an X-linked dosage compensation, as the
176 bx^{MS1096}-*GAL4* driver is inserted on the fly X chromosome [43,44].

177 Next, we measured the total adult wing area and lengths of six veins (longitudinal L2, L3,
178 L4, L5, ACV, and posterior crossvein or PCV) in the adult wing for each of the tested RNAi
179 lines that did not show lethality (or severe wrinkled phenotypes for vein length measurements)

180 (**Fig. 4A**). Overall, we identified significant wing measurement changes for 89 RNAi lines
181 compared to controls, which included lines that did not have an observable qualitative wing
182 phenotype (**Fig. 2C**). A summary of L3 vein lengths is presented in **Fig. 4B**, and the
183 measurements for the remaining five veins are provided in **S2 Fig.** and **S3 Data**. We found that
184 33/61 of the homologs (54.1%) showed significant changes in L3 vein length, including 20
185 homologs with longer vein lengths and 13 homologs with shorter vein lengths (**S4 Data**).
186 Additionally, 41/74 of the fly homologs (55.4%) showed changes in wing area (**S4 Data**),
187 including 36 homologs which showed smaller wing areas and five homologs showed larger wing
188 areas compared to controls (**S4 Data**). For example, both homologs of genes within 1q21.1
189 region, *BCL9*/*lgs* and *FMO5/Fmo-2*, showed decreased wing area and vein length, potentially
190 mirroring the reduced body length phenotype observed in mouse models of the deletion [45]
191 (**Fig. 4B-C**). In addition, *PAK2/Pak* within 3q29*, TBX1/org-1* within 22q11.2, autism-associated
192 *CHD8/kis*, and microcephaly-associated *ASPM/asp* also showed smaller wing areas and vein
193 lengths (**Fig. 4B-C**). In contrast, *TRPM1/Trpm* within 15q13.3 and the cell proliferation gene
194 *PTEN/Pten* [46] both showed larger wing areas and vein lengths (**Fig. 4B-C**). Furthermore, we
195 identified eight homologs that showed no qualitative wing phenotypes but had significant
196 changes in wing areas and vein lengths (**S4 Data**), including *CCDC101/Sgf29* in distal 16p11.2*,*
197 *FMO5/Fmo-2, TRPM1/Trpm, DHRS11/CG9150* in 17q12, and *NSUN5/Nsun5* in 7q11.23 (**Fig.**
198 **4B-C; S4 Data**). These results indicate that homologs of certain CNV genes may influence
199 variations in size without causing adverse wing phenotypes, and may be specifically implicated
200 towards cellular growth mechanisms.
201
202

203 **Homologs of CNV genes show global and tissue-specific effects during development**

204 We previously showed that many fly homologs of CNV genes that showed wing defects in the
205 current study also contributed towards neuronal phenotypes in the fly eye [30,31], suggesting a
206 role for these genes in global development. We therefore performed ubiquitous and eye-specific
207 knockdown of fly homologs to assess tissue-specific effects in comparison to the wing
208 phenotypes. First, we used the *da-GAL4* driver at 25°C to drive ubiquitous knockdown of RNAi
209 lines for 31 homologs of CNV genes, including 19 that were previously published [30,31]. We
210 observed complete or partial lethality at larval and pupal stages with knockdown of 10/31
211 homologs (32.3%) (**Fig. 5A**). Lethal phenotypes have also been documented for 43/130
212 knockout mouse models of individual CNV genes as well as for the entire deletion (**S5 Data**).
213 For example, mouse models heterozygous for the 16p11.2 deletion showed partial neonatal
214 lethality, while knockout mouse models of four individual genes within the 16p11.2 region,
215 including *Ppp4C*$^{-/-}$ and *Kif22*$^{-/-}$, showed embryonic lethality [14,47,48]. In our study, the
216 *DLG1/dlg1* line that showed lethality with wing-specific knockdown also exhibited larval
217 lethality with ubiquitous knockdown, indicating its role in global development (**Fig. 5A**). In
218 addition, six homologs that showed severe wing phenotypes also showed larval or pupal lethality
219 with ubiquitous knockdown, including *ALDOA/Ald* and *PPP4C/Pp4-19C* within 16p11.2 and
220 *ATXN2L/Atx2* and *TUFM/mEFTu1* within distal 16p11.2 (**Fig. 5A**). The remaining homologs
221 that showed lethality with ubiquitous knockdown showed at least a mild qualitative or
222 quantitative wing phenotype.

223 We next compared the phenotypes observed with wing-specific knockdown of fly
224 homologs to their corresponding eye-specific knockdowns to evaluate tissue-specific effects. The
225 *Drosophila* eye has been classically used to evaluate neuronal phenotypes due to genetic

226 perturbations, as individual ommatidial units within the eye contain photoreceptor neurons that
227 project into the optic lobe within the brain [49,50]. In fact, numerous genes associated with
228 human neurological disorders have been modeled using the fly eye [51–53]. To quantitatively
229 assess the phenotypic severity of cellular defects with eye-specific knockdown of fly homologs,
230 we developed a tool called *Flynotyper* [54] that quantifies the degree of disorganization among
231 the ommatidia in the adult eye. We analyzed phenotypic scores obtained from *Flynotyper* for 66
232 RNAi lines of 45 fly homologs, including from previously-published datasets [30,31,54]. We
233 found that 37/45 homologs (82.2%) exhibited both eye and wing-specific defects (**Fig. 5B, S3**
234 **Fig., S6 Data**). Two homologs with significant eye phenotypes did not show any wing
235 phenotypes, including *SPNS1/spin* within distal 16p11.2 and microcephaly-associated
236 *SLC25A19/Tpc1* [55], while five homologs only showed wing-specific phenotypes, including
237 *CDIPT/Pis* and *YPEL3/CG15309* within 16p11.2, *FBXO45/Fsn* and *OSTalpha/CG6836* within
238 3q29, and *UQCRC2/UQCR-C2* (**Fig. 5B, S3 Fig.**). In particular, *UQCRC2/UQCR-C2* showed
239 lethality with wing-specific knockdown, suggesting potential tissue-specific effects of this gene
240 in non-neuronal cells (**Fig. 5B**). While most homologs contributed towards both eye and wing-
241 specific phenotypes, we observed a wide range of severity in eye phenotypes that did not
242 correlate with the severity of quantitative or qualitative wing phenotypes (**Fig. 5C**). For example,
243 *TUFM/mEFTu1* showed a severe wing phenotype but only a mild increase in eye phenotypic
244 score, while *SH2B1/Lnk,* also within the distal 16p11.2 region, showed severe rough eye
245 phenotypes but only a mild increase in wing size (**Fig. 5D**). Similarly, *BCL9/lgs* also showed
246 opposing tissue-specific effects with mild qualitative wing phenotypes and severe eye
247 phenotypes, suggesting that the role of these homologs towards development differs across tissue
248 types.

249 **CNV genes show variable expression across different tissues in flies and humans**

250 To assess how expression levels of CNV genes vary across different tissues, we first examined
251 the expression patterns of fly homologs in larval and adult tissues using the FlyAtlas Anatomical
252 Microarray dataset [56]. We found that 76/77 homologs with available data were expressed in at
253 least one larval and adult tissue (**S4 Fig., S7 Data**). In general, we did not observe a correlation
254 between wing phenotype severity and expression patterns of homologs in larval or adult tissues
255 (**Fig. 6A**). For example, 58/77 homologs (75.3%) showed ubiquitous larval expression, including
256 both fly homologs that showed no qualitative wing phenotypes, such as *KCTD13/CG10465*
257 within 16p11.2 and *FBXO45/Fsn*, and those with severe wing phenotypes, such as *PPP4C/Pp4-*
258 *19C* and *NCBP2/Cbp20* (**Fig. 6A, S4 Fig.**). Furthermore, 30/39 homologs (76.9%) that showed
259 eye phenotypes also had ubiquitous larval expression, providing further support to the
260 observation that genes causing neuronal phenotypes may also contribute to developmental
261 phenotypes in other tissues (**S6 Data**). Of note, 9/77 homologs (11.7%) did not have any
262 expression in the larval central nervous system, including *FMO5/Fmo-2*, *BDH1/CG8888* within
263 3q29, and *TBX6/Doc2* within 16p11.2 (**Fig. 6A, S4 Fig.**). However, we observed wing
264 phenotypes for 8/9 of these homologs, suggesting that they may contribute to tissue-specific
265 phenotypes outside of the nervous system. Except for the epilepsy-associated *SCN1A/para* [57],
266 which was exclusively expressed in both the larval central nervous system (CNS) and adult brain
267 tissues, other tested neurodevelopmental genes were also expressed in non-neuronal tissues (**Fig.**
268 **6A**).

269 We further used the GTEx Consortium dataset [58] to examine tissue-specific expression
270 of 130 human CNV genes and 20 known neurodevelopmental genes across six tissues including
271 brain, heart, kidney, lung, liver, and muscle. We found 121/150 genes (80.7%) that were

272 expressed in at least one adult tissue, including 49/150 genes (32.7%) that showed ubiquitous
273 expression across all six tissues (**S6 Data**). Furthermore, 112/150 genes (74.7%) were expressed
274 in non-neuronal tissues, including 34/150 (22.7%) genes without any neuronal expression, such
275 as *TBX1*, *FMO5* and *GJA5* within 1q21.1, and *ATP2A1* within distal 16p11.2 (**Fig. 6B**, **S7 Data**).
276 *FMO5* and *TBX1* also showed non-neuronal expression in *Drosophila* tissues, suggesting that
277 their tissue-specific expression is highly conserved (**Fig. 6A**). Other genes with ubiquitous
278 expression also showed preferentially higher expression within specific non-neuronal tissues,
279 including *ALDOA* and *UQCRC2* for muscle and heart (**Fig. 6B**). In contrast, we found nine genes
280 that were expressed only in the adult brain, including *FAM57B* and *DOC2A* within 16p11.2, as
281 well as *SCN1A*, which showed similar CNS-only expression in *Drosophila* tissues (**Fig. 6B**, **S7**
282 **Data**).
283

284 **Knockdown of fly homologs of CNV genes lead to disruption of cellular processes**

285 Disruptions of basic cellular processes in neuronal cells, such as cell proliferation and apoptosis,
286 have been implicated in neurodevelopmental disorders [59–61]. We previously identified defects
287 in cell proliferation among photoreceptors neurons in larval eye discs with knockdown of
288 16p11.2 homologs, as well as increased apoptosis with knockdown of a subset of 3q29 homologs
289 [30,31]. Here, we explored how these basic cellular processes are altered in non-neuronal cells,
290 specifically in the developing wing disc, with knockdown of homologs of CNV genes. We
291 targeted 27 fly homologs that showed a range of adult wing phenotypes for changes in cell
292 proliferation and apoptosis, using immunostaining for anti-phospho-Histone H3 Ser10 (pH3) and
293 anti-*Drosophila* caspase-1 (dcp1), respectively, in the third instar larval wing discs. We
294 identified 23/27 homologs that showed significant increases in apoptotic cells compared to

295 controls, including seven homologs, such as *PPP4C/Pp4-19C*, *ATXN2L/Atx2*, and *AATF/Aatf* ,
296 which showed dcp1 staining across the entire larval wing pouch (**Fig. 7A-B, S5-S6 Figs., S8**
297 **Data**). In addition, 16/27 homologs showed decreased levels of proliferation, including eight
298 homologs which also showed apoptosis defects, such as *CYFIP1/Sra-1* within 15q11.2,
299 *SH2B1/Lnk*, and the microcephaly gene *KIF11/Klp61F* (**Fig. 7A and 7C, S5-S6 Figs., S8 Data**).
300 All six of the tested homologs with severe adult wing phenotypes showed both increased
301 apoptosis and decreased proliferation (**S8 Data**). Similarly, 3/4 homologs showing lethality with
302 wing-specific knockdown also showed defects in apoptosis or proliferation, with the exception of
303 *ACACA/ACC* (**S5 Fig.**, **S8 Data**). As bx^{MS1096}-*GAL4* is located on the X-chromosome, we
304 expected to see more severe defects in males compared with females due to the X-linked dosage
305 compensation [43,44]. However, knockdown of 3/11 tested homologs with sex-specific
306 differences in adult wing phenotypes, including *BCL9/lgs*, *CYFIP1/Sra-1*, and
307 *DNAJC30/CG11035* within 7q11.23, showed significantly decreased levels of cell proliferation
308 in females but no changes for males compared to their respective controls, suggesting sex-
309 specific effects of these genes towards cell proliferation (**S6 Fig., S8 Data**). Overall, our results
310 suggest that cell proliferation and apoptosis are disrupted by reduced expression of homologs of
311 CNV genes in both neuronal and non-neuronal tissues.
312

313 **Knockdown of homologs of CNV genes disrupt conserved signaling pathways**

314 Several conserved signaling pathways that are active in a spatial and temporal manner in the
315 larval wing disc, such as Wnt, Hedgehog, BMP, and Notch signaling, regulate the anterior-
316 posterior (A/P) and dorsal-ventral (D/V) boundaries to determine accurate morphology and vein
317 patterning in the adult wing [37,38,62–64]. For example, Wnt and Notch signaling pathways act

318 along the D/V boundary to determine cell fate [65,66], while Hedgehog signaling is dependent
319 upon expression of both engrailed in the posterior compartment and patched along the A/P
320 border [67,68]. Furthermore, O'Roak and colleagues showed that genes identified from *de novo*
321 mutations in patients with autism are linked to β-catenin/Wnt pathway [69]. In addition, familial
322 loss-of-function mutations in the human hedgehog signaling pathway gene *PTCH1* are
323 implicated in basal cell nevus syndrome, leading to basal cell carcinoma [70,71].

324 Based on adult wing phenotypes and disruptions to cellular processes, we next tested
325 whether knockdown of 14 fly homologs disrupt conserved signaling pathways in the third instar
326 larval wing disc (**S8 Data**). In particular, we evaluated the role of Wnt, Hedgehog, and Notch
327 signaling pathways by testing the expression patterns of four key proteins within these pathways,
328 including wingless (Wnt), patched (Hedgehog), engrailed (Hedgehog), and delta (Notch). We
329 found that 9/14 homologs, including 8/10 homologs showing severe wing phenotypes or
330 lethality, exhibited disruptions in at least one signaling pathway. For example, five homologs
331 with severe or lethal phenotypes showed disruptions of all four signaling pathways, including
332 *AATF/Aatf*, *NCBP2/Cbp20*, *POLR3E/Sin*, *PPP4C/Pp4-19C*, and *KIF11/Klp61F* (**Fig. 8, S8**
333 **Data**). Our observations are in concordance with previous findings by Swarup and colleagues,
334 who showed that *PPP4C/Pp4-19C* is a candidate regulator of Wnt and Notch signaling pathways
335 in *Drosophila* larval wing discs [72]. Furthermore, two genes from the 3q29 region, *DLG1/dlg1*
336 and *MFI2/Tsf2*, showed altered expression patterns for delta and patched but not for engrailed,
337 indicating that they selectively interact with the Hedgehog as well as Notch signaling pathway
338 (**S7 Fig.**). In fact, Six and colleagues showed that Dlg1 directly binds to the PDZ-binding domain
339 of Delta1 [73]. In contrast, *ACACA/ACC* and *UQCRC2/UQCR-C2* showed no changes in
340 expression patterns for any of the four signaling proteins tested, suggesting that the observed

341 lethality could be due to other cellular mechanisms (**S7 Fig.**). We conclude that several
342 homologs disrupt the expression of key proteins in signaling pathways in the developing larval
343 wing discs, potentially accounting for the developmental defects observed in the adult wings.
344

345 **Connectivity patterns of CNV genes vary across human tissue-specific networks**

346 We examined patterns of connectivity for nine candidate genes, based on disruptions of signaling
347 pathways identified in developing *Drosophila* wing discs, within the context of human brain,
348 heart, and kidney-specific gene interaction networks [74]. These tissue-specific networks were
349 constructed using Bayesian classifier-generated probabilities for pairwise genetic interactions
350 based on co-expression data [74]. Within each network, we calculated the lengths of the shortest
351 paths between each candidate gene and 267 genes from the Wnt, Notch, and Hedgehog pathways
352 as a proxy for connectivity (**S9 Data**). In all three networks, each of the candidate genes were
353 connected to a majority of the signaling pathway genes (**Fig. 9A, S8 Fig.**). Interestingly, we
354 observed a higher connectivity (i.e. shorter path distances) between candidate genes and Wnt and
355 Hedgehog pathway genes in the brain-specific network compared to the heart and kidney-
356 specific networks (**Fig. 9B**). We further identified enrichments for genes involved in specific
357 biological processes among the connector genes that were located in the shortest paths within
358 neuronal and non-neuronal tissue-specific networks (**Fig. 9C, S9 Data**). For example, axon-
359 dendrite transport, dopaminergic signaling, and signal transduction functions were enriched
360 among connector genes only for the brain-specific network, while organelle organization and
361 protein ubiquitination were enriched among connector genes only for kidney and heart networks
362 (**Fig. 9C**). However, several core biological processes, such as cell cycle, protein metabolism,
363 transcriptional regulation, and RNA processing/splicing, were enriched among connector genes

364 within all three tissue-specific networks (**Fig. 9C**). Our analysis highlights that human CNV
365 genes potentially interact with developmental signaling pathways in a ubiquitous manner, but
366 may affect different biological processes in neuronal and non-neuronal tissues.

367 **DISCUSSION**

368 We used the *Drosophila* wing as a model to assess how homologs of key CNV genes contribute
369 towards non-neuronal phenotypes. We tested fly homologs of 79 genes and identified multiple
370 homologs within each CNV region that exhibited robust phenotypes indicative of developmental
371 disruptions. Several themes have emerged from our study highlighting the importance of fly
372 homologs of CNV genes towards both global and tissue-specific phenotypes.

373 *First*, we found that fly homologs of CNV genes contribute towards developmental
374 phenotypes through ubiquitous roles in neuronal and non-neuronal tissues. Although we did not
375 study models for the entire CNV, nearly all individual fly homologs of CNV genes contribute to
376 wing-specific developmental defects. It is likely that these genes also contribute to additional
377 phenotypes in other tissues that we did not assess. In fact, a subset of these homologs also
378 showed early lethality with ubiquitous knockdown in addition to severe or lethal wing-specific
379 phenotypes. However, we found no correlation between the severity of the eye and wing
380 phenotypes, suggesting tissue-specific effects of these homologs towards developmental defects.
381 In contrast, fly homologs of known neurodevelopmental genes generally showed milder wing
382 phenotypes compared with eye phenotypes, indicating a more neuronal role for these genes.
383 While our study only examined a subset of CNV genes with *Drosophila* homologs, phenotypic
384 data from knockout mouse models also support a global developmental role for individual CNV
385 genes. In fact, 44/130 (33.8%) knockout models of CNV genes within the Mouse Genome
386 Informatics (MGI) database [75] exhibited non-neuronal phenotypes, including 20 homologs of
387 CNV genes that showed both neuronal and non-neuronal phenotypes (**S5 Data**). For example,
388 knockout mouse models of *Dlg1*$^{-/-}$ showed defects in dendritic growth and branching in the
389 developing nervous system, in addition to craniofacial features and multiple kidney and urinary

390 tract defects [76–79]. Furthermore, Chapman and colleagues showed that knockout of *Tbx6*$^{-/-}$
391 caused defects in mesodermal and neuronal differentiation early in development, leading to
392 abnormal vascular, tail bud, and neural tube morphology [80]. These observations further
393 support our findings that most fly homologs of CNV genes have a global role in development
394 that could account for the observed non-neuronal defects.

395 *Second*, based on tissue-specific phenotypes, we identified fly homologs of CNV genes
396 that are key regulators of conserved cellular processes important for development. For example,
397 9/10 homologs with severe or lethal adult wing phenotypes also exhibited defects in cell
398 proliferation and apoptosis during development. In fact, we found concordance between cellular
399 processes affected by wing and eye-specific knockdown of homologs of genes within 16p11.2
400 and 3q29 regions, including decreased proliferation for *MAPK3/rl* and increased apoptosis for
401 *NCBP2/Cbp20* and *DLG1/dlg1* [30,31]. While eye-specific knockdown of *BDH1/CG8888*
402 showed decreased cell proliferation in larval eye discs [31], we found increased cell proliferation
403 with wing-specific knockdown, suggesting a tissue-specific effect for this gene. Notably, at least
404 one fly homolog per CNV region showed defects in cell proliferation or apoptosis, suggesting
405 these cellular processes are important for development in both neuronal and non-neuronal
406 tissues. For example, *ATXN2L/Atx2*, *SH2B1/Lnk*, and *CCDC101/Sgf29* each showed decreased
407 proliferation and increased apoptosis, suggesting a potential shared cellular mechanism for
408 several genes within the distal 16p11.2 deletion. Furthermore, a subset of these genes also
409 disrupted multiple signaling pathways, indicating a potential role for these homologs as key
410 regulators of developmental processes. We specifically identified five homologs whose
411 knockdown caused disruptions of Wnt, Notch, and hedgehog signaling pathways. Each of these
412 genes have important roles in cell cycle regulation, apoptosis, transcription, or RNA processing,

413 based on Gene Ontology annotations [81,82]. In fact, we found that the RNA transport protein
414 *NCBP2/Cbp20* [83], which we recently identified as a key modifier gene for the 3q29 deletion
415 [31], interfaced with all three signaling pathways. Furthermore, *AATF* disrupts apoptosis and
416 promotes cell cycle progression through displacement of HDAC1 [84–86], while *PPP4C*
417 promotes spindle organization at the centromeres during mitosis [87]. While we only evaluated
418 the role of these genes towards development in a single fly tissue, our additional analysis of
419 human gene interaction networks showed strong connectivity between the CNV genes and
420 signaling pathways in multiple neuronal and non-neuronal human tissues. In fact, cell cycle
421 genes were enriched among the connector genes in all three tested tissue-specific networks,
422 further emphasizing the role of cell cycle processes towards developmental phenotypes. Notably,
423 we also observed certain biological processes enriched among connector genes that were specific
424 to neuronal or non-neuronal tissues, indicating that genes within CNV regions may affect
425 different biological processes in a tissue-specific manner.

426 *Overall*, we show that fly homologs of most CNV genes contribute towards global
427 developmental phenotypes, although exactly how they contribute toward such phenotypes varies
428 between neuronal and non-neuronal tissues. Previous functional studies for CNV disorders have
429 focused primarily on identifying candidate genes for the observed neuronal phenotypes. In this
430 study, we identified several homologs of CNV genes that are responsible for non-neuronal
431 defects, as well as novel associations between these homologs and conserved biological
432 processes and pathways. We therefore propose that multiple genes within each CNV region
433 differentially disrupt conserved cellular pathways and biological processes in neuronal versus
434 non-neuronal tissues during development (**Fig. 10**). These results are in line with a multigenic
435 model for CNV disorders, as opposed to models where individual causative genes are

436 responsible for specific phenotypes [30,31,88]. Our study further exemplifies the utility of
437 evaluating non-neuronal phenotypes in addition to neuronal phenotypes in functional models of
438 individual genes and CNV regions associated with developmental disorders, including future
439 studies in mammalian or cellular model systems. Further studies exploring how CNV genes
440 interact with each other and with other developmental pathways could more fully explain the
441 conserved mechanisms underlying global developmental defects and identify potential
442 therapeutic targets for these disorders.
443

MATERIALS AND METHODS

Fly stocks and genetics

We selected *Drosophila* homologs for 59 human genes out of 130 total genes located within 10 pathogenic CNV regions [89] associated with neurodevelopmental disorders (1q21.1, 3q29, 7q11.23, 15q11.2, 15q13.3, 16p11.2, distal 16p11.2, 16p12.1, 16p13.11, and 17q12) (**S2 Data**). These 59 genes were selected based on presence of fly homologs, availability of RNAi lines for fly homologs, and quality control of the RNAi lines. In addition, we evaluated fly homologs of 20 human genes known to be in involved in neurodevelopmental disorders [54,90] (**S2 Data**). These include genes involved in beta-catenin signaling pathway (5 genes), core genes implicated in neurodevelopmental disorders (8 genes), and genes associated with microcephaly (7 genes) [91]. We note that 2/20 neurodevelopmental genes, *TBX1* (22q11.2 deletion) [92] and *UBE3A* (Prader-Willi/Angelman syndrome region) [93], are located within other pathogenic CNV regions. We used the DRSC Integrative Ortholog Prediction Tool (DIOPT, v.7.1) [42] to select fly homologs for each human gene based on highest numeric score, excluding genes with "low" rankings (score <2) (**S2 Data**).

To knockdown individual genes in specific tissues, we used RNA interference (RNAi) and the *UAS-GAL4* system (**Fig. 1**), a well-established tool that allows for tissue-specific expression of a gene of interest [94]. RNAi lines were obtained from Vienna *Drosophila* Resource Center (VDRC) that include both GD and KK lines. We tested a total of 136 lines in our final data analysis (**S10 Data**). A complete list of stock numbers and full genotypes for all RNAi lines used in this study is presented in **S10 Data**. We used the bx^{MS1096}*-GAL4/FM7c;;UAS-Dicer2/TM6B* driver for wing-specific knockdown and w^{1118}*;GMR-GAL4*;*UAS-Dicer2* driver (Claire Thomas, Penn State University) for eye-specific knockdown of RNAi lines. Ubiquitous

467 knockdown experiments were performed using the *w;da-GAL4;+* driver (Scott Selleck, Penn
468 State University). For all experiments, we used appropriate GD (w^{1118}, VDRC# 60000) or KK
469 ($y,w^{1118}; P\{attP,y^{+},w^{3`}\}$, VDRC# 60100) lines as controls to compare against lines with
470 knockdown of individual homologs. All fly lines were reared on standard yeast *Drosophila*
471 medium at room temperature. All crosses were set and maintained at 25°C, except for the eye
472 knockdown experiments which were maintained at 30°C.
473

474 **Phenotypic analysis of adult wing images**

475 Adult progeny were isolated from crosses between RNAi lines and bx^{MS1096}-*GAL4* driver shortly
476 after eclosion, and kept at 25°C until day 2-5 (**Fig. 1**). At that point, the progeny were frozen at -
477 80°C, and were then moved to -20°C prior to imaging and storage. Approximately 20-25
478 progeny, both male and female, were collected for each RNAi line tested. The adult wings were
479 plucked from frozen flies and mounted on a glass slide. The slides were covered with a coverslip
480 and sealed using clear nail polish. Adult wing images were captured using a Zeiss Discovery
481 V20 stereoscope (Zeiss, Thornwood, NY, USA), with a ProgRes Speed XT Core 3 camera and
482 CapturePro v.2.8.8 software (Jenoptik AG, Jena, Germany) at 40X magnification.

483 For each non-lethal RNAi line, we scored the adult wing images for five qualitative
484 phenotypes, including wrinkled wing, discoloration, missing veins, ectopic veins, and bristle
485 planar polarity defects, on a scale of 1 (no phenotype) to 5 (lethal) (**Fig. 3C**). Lines showing
486 severely wrinkled wings or lethality were scored as 4 (severe) or 5 (lethal) for all five
487 phenotypes. We calculated the frequency of each phenotypic score (i.e. mild bristle polarity,
488 moderate discoloration) across all of the wing images for each line (**Fig. 3A-B**, **S3 Data**), and
489 then performed k-means clustering of values for female RNAi lines to generate five clusters for

490 overall wing phenotypes (**Fig. 2B**, **S3 Data**). For quantitative analysis of wing phenotypes, we
491 used the Fiji ImageJ software [95] to calculate the wing area using the Measure Area tool, and
492 calculated the lengths of longitudinal veins L2, L3, L4, and L5 as well as the anterior and
493 posterior crossveins (ACV and PCV) by tracing individual veins using the Segmented Line tool
494 (**Fig. 4A, S3 Data**). We determined discordant homologs when multiple RNAi lines for the same
495 homolog showed no wing phenotype versus any qualitative or quantitative wing phenotypes,
496 followed by discordance for small or large wing measurement phenotypes (**S4 Data**).
497

498 **Phenotypic analysis of adult eye images**

499 We crossed RNAi lines with *GMR-GAL4* to achieve eye-specific knockdown of homologs of
500 CNV and known neurodevelopmental genes. Adult 2-3-day old female progenies from the
501 crosses were collected, immobilized by freezing at -80°C, and then moved to -20°C prior to
502 imaging and storage. Flies were mounted on Blu-tac (Bostik Inc, Wauwatosa, WI, USA) and
503 imaged using an Olympus BX53 compound microscope with LMPLan N 20X air objective using
504 a DP73 c-mount camera at 0.5X magnification (Olympus Corporation, Tokyo, Japan). CellSens
505 Dimension software (Olympus Corporation, Tokyo, Japan) was used to capture the eye images,
506 which were then stacked using the Zerene Stacker software (Zerene Systems LLC, Richland,
507 WA, USA). All eye images presented in this study are maximum projections of 20 consecutive
508 optical z-sections, at a z-step size of 12.1µm. Finally. we used our computational method called
509 *Flynotyper* (https://flynotyper.sourceforge.net) to quantify the degree of rough eye phenotypes
510 present due to knockdown of homologs of CNV or neurodevelopmental genes [54]. *Flynotyper*
511 scores for homologs of 16p11.2 and 3q29, as well as select core neurodevelopmental genes, were
512 derived from our previous studies [30,31,54].

513

514 **Immunohistochemistry**

515 Wing imaginal discs from third instar larvae were dissected in 1X PBS. The tissues were fixed
516 using 4% paraformaldehyde and blocked using 1% bovine serum albumin (BSA). The wing discs
517 were incubated with primary antibodies using appropriate dilutions overnight at 4°C. We used
518 the following primary antibodies: mouse monoclonal anti-pHistone3 (S10) (1:100 dilutions, Cell
519 Signaling 9706L), rabbit polyclonal anti-cleaved *Drosophila* Dcp1 (Asp216) (1:100 dilutions,
520 Cell Signaling 9578S), mouse monoclonal anti-wingless (1:200 dilutions, DSHB, 4D4), mouse
521 monoclonal anti-patched (1:50 dilutions, DSHB, *Drosophila* Ptc/APA1), mouse monoclonal
522 anti-engrailed (1:50 dilutions, DSHB, 4D9), and mouse monoclonal anti-delta (1:50 dilutions,
523 DSHB, C594.9B). Following incubation with primary antibodies, the wing discs were washed
524 and incubated with secondary antibodies at 1:200 dilution for two hours at room temperature.
525 We used the following secondary antibodies: Alexa Fluor 647 dye goat anti-mouse (A21235,
526 Molecular Probes by Invitrogen/Life Technologies), Alexa Fluor 568 dye goat anti-rabbit
527 (A11036, Molecular Probes by Invitrogen/Life Technologies), and Alexa Fluor 568 dye goat
528 anti-mouse (A11031, Molecular Probes by Invitrogen/Life Technologies). All washes and
529 antibody dilutions were made using 0.3% PBS with Triton-X.

530 Third instar larvae wing imaginal discs were mounted in Prolong Gold antifade reagent
531 with DAPI (Thermo Fisher Scientific, P36930) for imaging using an Olympus Fluoview FV1000
532 laser scanning confocal microscope (Olympus America, Lake Success, NY). Images were
533 acquired using FV10-ASW 2.1 software (Olympus, Waltham, MA, USA). Composite z-stack
534 images were analyzed using the Fiji ImageJ software [95]. To calculate the number of pH3
535 positive cells within the wing pouch area of the wing discs, we used the AnalyzeParticles

536 function in ImageJ, while manual counting was used to quantify Dcp1 positive cells. We note
537 that cell proliferation and apoptosis staining for *NCBP2/Cbp20*, *DLG1/dlg1*, *BDH1/CG8888*, and
538 *FBXO45/Fsn* were previously published[31].
539
540 **Statistical analysis**
541 Significance for the wing area and vein length measurements, cell counts for proliferation and
542 apoptosis, and *Flynotyper* scores were compared to appropriate GD or KK controls using one-
543 tailed or two-tailed Mann-Whitney tests. P-values for each set of experiments were corrected for
544 multiple testing using Benjamini-Hochberg correction. All statistical and clustering analysis was
545 performed using R v.3.6.1 (R Center for Statistical Computing, Vienna, Austria). Details for the
546 statistical tests performed for each dataset are provided in **S11 Data**.
547
548 **Expression data analysis**
549 We obtained tissue-specific expression data for fly homologs of CNV genes from the FlyAtlas
550 Anatomical Microarray dataset [56]. Raw FPKM (fragments per kilobase of transcript per
551 million reads) expression values for each tissue were categorized as follows: <10, no expression;
552 10-100, low expression; 100-500, moderate expression; 500-1000, high expression; and >1000,
553 very high expression (**S7 Data**). The median expression among midgut, hindgut, Malpighian
554 tube, and (for adult only) crop tissues was used to represent overall gut expression. We similarly
555 obtained human tissue-specific expression data for CNV genes from the GTEx Consortium v.1.2
556 RNA-Seq datasets [58]. Median TPM (transcripts per million reads) expression values for each
557 tissue were categorized as follows: <3, no expression; 3-10, low expression; 10-25, moderate
558 expression; 25-100, high expression; and >100, very high expression (**S7 Data**). The median

559 expression among all brain and heart sub-tissues was used to represent brain and heart
560 expression, while the median expression among all colon, esophagus, small intestine, and
561 stomach sub-tissues was used to represent digestive tract expression. Tissue-specific preferential
562 gene expression was determined if the expression of a gene within a particular tissue was greater
563 than the third quartile of expression values for that gene across all tissues, plus 1.5 times the
564 interquartile range. Venn diagrams were generated using the Venny webtool
565 (http://bioinfogp.cnb.csic.es/tools/venny) (**S4 Fig.**).
566

567 **Network analysis**

568 We obtained human tissue-specific gene interaction networks for brain, heart, and kidney tissues
569 from the GIANT network database [74] within HumanBase (https://hb.flatironinstitute.org).
570 These networks were built using a Bayesian classifier trained on tissue-specific gene co-
571 expression datasets, which assigned posterior probabilities for interactions between pairs of
572 genes within a particular tissue. We downloaded the "Top edge" version of each tissue-specific
573 network, and extracted all gene pairs with posterior probabilities >0.2 to create sub-networks
574 containing the top ~0.5% tissue-specific interactions. Next, we identified the shortest paths in
575 each sub-network between human CNV genes whose fly homologs disrupted signaling pathways
576 in the larval wing disc and human genes within each disrupted pathway, using the inverse of the
577 posterior probabilities as weights for each edge in the network. Gene sets from the human Notch
578 (KEGG:map04330), Wnt (KEGG:map04310) and Hedgehog pathways (KEGG:map04340) were
579 curated from the Kyoto Encyclopedia of Genes and Genomes (KEGG) pathway database [96].
580 Using the NetworkX Python package [97], we calculated the shortest distance between each
581 CNV gene and pathway gene, and identified connecting genes that were within each of the

582 shortest paths for the three tissue-specific networks. We further tested for enrichment of Gene
583 Ontology (GO) terms (PantherDB GO-Slim) among the connector genes using the PantherDB
584 Gene List Analysis tool [98]. Lists of the shortest paths and connector genes in each tissue-
585 specific network, as well as enriched GO terms for sets of connector genes, are provided in **S9**
586 **Data**. Gene networks were visualized in Cytoscape v.3.7.2 [99] using an edge-weighted spring
587 embedded layout.
588

589 **Mouse and human phenotypic data analysis**

590 Phenotypic data for mouse models of CNV gene homologs, categorized using top-level
591 Mammalian Phenotype Ontology terms, were obtained from the Mouse Genome Informatics
592 (MGI) database [75] (**S5 Data**). Phenotypic data for human carriers of 10 pathogenic CNVs were
593 obtained from the DECIPHER public database [9] (**S1 Data**). Clinical phenotypes for each CNV
594 carrier were categorized by top-level Human Phenotype Ontology terms [100] using the Orange3
595 Bioinformatics software library (https://orange-bioinformatics.readthedocs.io), and the frequency
596 of individuals carrying each top-level phenotype term was calculated for each CNV.
597

598 **Data availability**

599 All data supporting the findings of this study are available within the paper and its
600 supplementary data files. All source code for data analysis in this manuscript, including scripts
601 for k-means clustering of fly phenotypes, network connectivity of CNV and developmental
602 pathway genes, and extraction of top-level human phenotype terms, are available on the
603 Girirajan lab GitHub page at https://github.com/girirajanlab/CNV_wing_project.
604

605 **ACKNOWLEDGEMENTS**

606 The authors thank Drs. Scott Selleck and Claire Thomas for providing fly lines for the
607 experiments, and members of the Girirajan Lab for their helpful discussions and comments on
608 the manuscript. This work was supported by NIH R01-GM121907 and resources from the Huck
609 Institutes of the Life Sciences to S.G., and NIH T32-GM102057 to M.J. This study makes use of
610 data generated by the DECIPHER community. A full list of centers who contributed to the
611 generation of the data is available from http://decipher.sanger.ac.uk and via email from
612 decipher@sanger.ac.uk. Funding for the DECIPHER project was provided by the Wellcome
613 Trust.

614

615 **CONTRIBUTIONS**

616 T.Y., M.J., S.Y., and S.G. designed the study. T.Y., S.Y., L.P., S.K., D.J.G., A.S., E.G., Y.M.,
617 J.I., and Z.C.L. performed the functional experiments. T.Y. and M.J. performed the expression
618 and network experiments. T.Y., M.J., and S.G. analyzed the data and wrote the manuscript with
619 input from all authors.

620

621 **COMPETING OF INTERESTS**

622 The authors declare that they have no competing interests.

623 **REFERENCES**
624

625 1. Girirajan S, Campbell CD, Eichler EE. Human Copy Number Variation and Complex
626 Genetic Disease. Annu Rev Genet. 2011;45: 203–226. doi:10.1146/annurev-genet-
627 102209-163544
628 2. Malhotra D, Sebat J. CNVs: harbingers of a rare variant revolution in psychiatric genetics.
629 Cell. 2012;148: 1223–1241. doi:10.1016/j.cell.2012.02.039
630 3. Cooper GM, Coe BP, Girirajan S, Rosenfeld JA, Vu TH, Baker C, et al. A copy number
631 variation morbidity map of developmental delay. Nat Genet. 2011;43: 838–846.
632 doi:10.1038/ng.909
633 4. Zhang F, Gu W, Hurles ME, Lupski JR. Copy Number Variation in Human Health,
634 Disease, and Evolution. Annu Rev Genomics Hum Genet. 2009;10: 451–481.
635 doi:10.1146/annurev.genom.9.081307.164217
636 5. Greenway SC, Pereira AC, Lin JC, Depalma SR, Israel SJ, Mesquita SM, et al. De novo
637 copy number variants identify new genes and loci in isolated sporadic tetralogy of Fallot.
638 Nat Genet. 2009;41: 931–935. doi:10.1038/ng.415
639 6. Glessner JT, Bick AG, Ito K et al. Increased Frequency of De Novo Copy Number
640 Variations in Congenital Heart Disease by Integrative Analysis of SNP Array and Exome
641 Sequence Data. Circ Res. 2014;115: 884–896. doi:10.1161/CIRCRESAHA.115.304458.
642 7. Sanna-Cherchi S, Kiryluk K, Burgess KE, Bodria M, Sampson MG, Hadley D, et al.
643 Copy-number disorders are a common cause of congenital kidney malformations. Am J
644 Hum Genet. 2012;91: 987–997. doi:10.1016/j.ajhg.2012.10.007
645 8. Zahnleiter D, Uebe S, Ekici AB, Hoyer J, Wiesener A, Wieczorek D, et al. Rare copy
646 number variants are a common cause of short stature. PLoS Genet. 2013;9: e1003365.
647 doi:10.1371/journal.pgen.1003365
648 9. Firth H V., Richards SM, Bevan AP, Clayton S, Corpas M, Rajan D, et al. DECIPHER:
649 Database of Chromosomal Imbalance and Phenotype in Humans Using Ensembl
650 Resources. Am J Hum Genet. 2009;84: 524–533. doi:10.1016/j.ajhg.2009.03.010
651 10. Mefford HC, Sharp AJ, Baker C, Itsara A, Jiang Z, Buysse K, et al. Recurrent
652 rearrangements of chromosome 1q21.1 and variable pediatric phenotypes. N Engl J Med.
653 2008;359: 1685–99. doi:10.1056/NEJMoa0805384
654 11. Brunetti-Pierri N, Berg JS, Scaglia F, Belmont J, Bacino CA, Sahoo T, et al. Recurrent
655 reciprocal 1q21.1 deletions and duplications associated with microcephaly or
656 macrocephaly and developmental and behavioral abnormalities. Nat Genet. 2008;40:
657 1466–1471. doi:10.1038/ng.279
658 12. Christiansen J, Dyck JD, Elyas BG, Lilley M, Bamforth JS, Hicks M, et al. Chromosome
659 1q21.1 contiguous gene deletion is associated with congenital heart disease. Circ Res.
660 2004;94: 1429–35. doi:10.1161/01.RES.0000130528.72330.5c
661 13. Pober BR. Williams-Beuren syndrome. N Engl J Med. 2010;362: 239–52.
662 doi:10.1056/NEJMra0903074
663 14. Horev G, Ellegood J, Lerch JP, Son Y-EE, Muthuswamy L, Vogel H, et al. Dosage-
664 dependent phenotypes in models of 16p11.2 lesions found in autism. Proc Natl Acad Sci.
665 2011;108: 17076–17081. doi:10.1073/pnas.1114042108
666 15. Pucilowska J, Vithayathil J, Tavares EJ, Kelly C, Karlo JC, Landreth GE. The 16p11.2
667 Deletion Mouse Model of Autism Exhibits Altered Cortical Progenitor Proliferation and

668 Brain Cytoarchitecture Linked to the ERK MAPK Pathway. J Neurosci. 2015;35: 3190–
669 3200. doi:10.1523/JNEUROSCI.4864-13.2015
670 16. Portmann T, Yang M, Mao R, Panagiotakos G, Ellegood J, Dolen G, et al. Behavioral
671 abnormalities and circuit defects in the basal ganglia of a mouse model of 16p11.2
672 deletion syndrome. Cell Rep. 2014;7: 1077–1092. doi:10.1016/j.celrep.2014.03.036
673 17. Rutkowski TP, Purcell RH, Pollak RM, Grewenow SM, Gafford GM, Malone T, et al.
674 Behavioral changes and growth deficits in a CRISPR engineered mouse model of the
675 schizophrenia-associated 3q29 deletion. Mol Psychiatry. 2019. doi:10.1038/s41380-019-
676 0413-5
677 18. Baba M, Yokoyama K, Seiriki K, Naka Y, Matsumura K, Kondo M, et al. Psychiatric-
678 disorder-related behavioral phenotypes and cortical hyperactivity in a mouse model of
679 3q29 deletion syndrome. Neuropsychopharmacology. 2019;44: 2125–2135.
680 doi:10.1038/s41386-019-0441-5
681 19. Arbogast T, Ouagazzal A-M, Chevalier C, Kopanitsa M, Afinowi N, Migliavacca E, et al.
682 Reciprocal Effects on Neurocognitive and Metabolic Phenotypes in Mouse Models of
683 16p11.2 Deletion and Duplication Syndromes. PLOS Genet. 2016;12: e1005709.
684 doi:10.1371/journal.pgen.1005709
685 20. Haller M, Au J, O'Neill M, Lamb DJ. 16p11.2 transcription factor MAZ is a dosage-
686 sensitive regulator of genitourinary development. Proc Natl Acad Sci. 2018;115:
687 201716092. doi:10.1073/pnas.1716092115
688 21. Yadav S, Oses-Prieto JA, Peters CJ, Zhou J, Pleasure SJ, Burlingame AL, et al. TAOK2
689 Kinase Mediates PSD95 Stability and Dendritic Spine Maturation through Septin7
690 Phosphorylation. Neuron. 2017;93: 379–393. doi:10.1016/j.neuron.2016.12.006
691 22. Richter M, Murtaza N, Scharrenberg R, White SH, Johanns O, Walker S, et al. Altered
692 TAOK2 activity causes autism-related neurodevelopmental and cognitive abnormalities
693 through RhoA signaling. Mol Psychiatry. 2019;24: 1329–1350. doi:10.1038/s41380-018-
694 0025-5
695 23. Golzio C, Willer J, Talkowski ME, Oh EC, Taniguchi Y, Jacquemont S, et al. KCTD13 is
696 a major driver of mirrored neuroanatomical phenotypes of the 16p11.2 copy number
697 variant. Nature. 2012;485: 363–367. doi:10.1038/nature11091
698 24. Escamilla CO, Filonova I, Walker AK, Xuan ZX, Holehonnur R, Espinosa F, et al.
699 Kctd13 deletion reduces synaptic transmission via increased RhoA. Nature. 2017;551:
700 227–231. doi:10.1038/nature24470
701 25. Ip JPK, Nagakura I, Petravicz J, Li K, Wiemer EAC, Sur M. Major vault protein, a
702 candidate gene in 16p11.2 microdeletion syndrome, is required for the homeostatic
703 regulation of visual cortical plasticity. J Neurosci. 2018;38: 2017–2034.
704 doi:10.1523/JNEUROSCI.2034-17.2018
705 26. Dickinson ME, Flenniken AM, Ji X, Teboul L, Wong MD, White JK, et al. High-
706 throughput discovery of novel developmental phenotypes. Nature. 2016;537: 508–514.
707 doi:10.1038/nature19356
708 27. Wangler MF, Yamamoto S, Bellen HJ. Fruit flies in biomedical research. Genetics.
709 2015;199: 639–653. doi:10.1534/genetics.114.171785
710 28. Chien S. Homophila: human disease gene cognates in Drosophila. Nucleic Acids Res.
711 2002;30: 149–151. doi:10.1093/nar/30.1.149
712 29. Reiter LT, Potocki L, Chien S, Gribskov M, Bier E. A systematic analysis of human

713 disease-associated gene sequences in Drosophila melanogaster. Genome Res. 2001;11:
714 1114–1125. doi:10.1101/gr.169101
715 30. Iyer J, Singh MD, Jensen M, Patel P, Pizzo L, Huber E, et al. Pervasive genetic
716 interactions modulate neurodevelopmental defects of the autism-associated 16p11.2
717 deletion in Drosophila melanogaster. Nat Commun. 2018;9: 2548. doi:10.1038/s41467-
718 018-04882-6
719 31. Singh MD, Jensen M, Lasser M, Huber E, Yusuff T, Pizzo L, et al. NCBP2 modulates
720 neurodevelopmental defects of the 3q29 deletion in Drosophila and Xenopus laevis
721 models. PLOS Genet. 2020;16: e1008590. doi:10.1371/journal.pgen.1008590
722 32. Molnar C, Resnik-Docampo M, F. M, Martin M, F. C, de Celis JF. Signalling Pathways in
723 Development and Human Disease: A Drosophila Wing Perspective. Human Genetic
724 Diseases. InTech; 2011. doi:10.5772/23858
725 33. Dworkin I, Gibson G. Epidermal growth factor receptor and transforming growth factor-β
726 signaling contributes to variation for wing shape in Drosophila melanogaster. Genetics.
727 2006;173: 1417–1431. doi:10.1534/genetics.105.053868
728 34. Testa ND, Dworkin I. The sex-limited effects of mutations in the EGFR and TGF-β
729 signaling pathways on shape and size sexual dimorphism and allometry in the Drosophila
730 wing. Dev Genes Evol. 2016;226: 159–171. doi:10.1007/s00427-016-0534-7
731 35. Yan SJ, Gu Y, Li WX, Fleming RJ. Multiple signaling pathways and a selector protein
732 sequentially regulate Drosophila wing development. Development. 2004;131: 285–298.
733 doi:10.1242/dev.00934
734 36. Strigini M, Cohen SM. A Hedgehog activity gradient contributes to AP axial patterning of
735 the Drosophila wing. Development. 1997;124: 4697–4705.
736 37. Diaz de la Loza MC, Thompson BJ. Forces shaping the Drosophila wing. Mech Dev.
737 2017;144: 23–32. doi:10.1016/j.mod.2016.10.003
738 38. Bier E. Drosophila, the golden bug, emerges as a tool for human genetics. Nat Rev Genet.
739 2005;6: 9–23. doi:10.1038/nrg1503
740 39. Wu Y, Bolduc F V, Bell K, Tully T, Fang Y, Sehgal A, et al. A Drosophila model for
741 Angelman syndrome. Proc Natl Acad Sci U S A. 2008;105: 12399–12404.
742 doi:10.1073/pnas.0805291105
743 40. Yamamoto S, Jaiswal M, Charng WL, Gambin T, Karaca E, Mirzaa G, et al. A drosophila
744 genetic resource of mutants to study mechanisms underlying human genetic diseases. Cell.
745 2014;159: 200–214. doi:10.1016/j.cell.2014.09.002
746 41. Kochinke K, Zweier C, Nijhof B, Fenckova M, Cizek P, Honti F, et al. Systematic
747 Phenomics Analysis Deconvolutes Genes Mutated in Intellectual Disability into
748 Biologically Coherent Modules. Am J Hum Genet. 2016;98: 149–164.
749 doi:10.1016/j.ajhg.2015.11.024
750 42. Hu Y, Flockhart I, Vinayagam A, Bergwitz C, Berger B, Perrimon N, et al. An integrative
751 approach to ortholog prediction for disease-focused and other functional studies. BMC
752 Bioinformatics. 2011;12: 357. doi:10.1186/1471-2105-12-357
753 43. Capdevila J, Guerrero I. Targeted expression of the signaling molecule decapentaplegic
754 induces pattern duplications and growth alterations in Drosophila wings. EMBO J.
755 1994;13: 4459–4468. doi:10.1002/j.1460-2075.1994.tb06768.x
756 44. Lindström R, Lindholm P, Palgi M, Saarma M, Heino TI. In vivo screening reveals
757 interactions between Drosophila Manf and genes involved in the mitochondria and the

758 ubiquinone synthesis pathway. BMC Genet. 2017;18: 52. doi:10.1186/s12863-017-0509-3
759 45. Nielsen J, Fejgin K, Sotty F, Nielsen V, Mørk A, Christoffersen CT, et al. A mouse model
760 of the schizophrenia-associated 1q21.1 microdeletion syndrome exhibits altered
761 mesolimbic dopamine transmission. Transl Psychiatry. 2017;7: 1261. doi:10.1038/s41398-
762 017-0011-8
763 46. Huang H, Potter CJ, Tao W, Li DM, Brogiolo W, Hafen E, et al. PTEN affects cell size,
764 cell proliferation and apoptosis during Drosophila eye development. Development.
765 1999;126: 5365–5372. doi:10.5167/uzh-627
766 47. Toyo-oka K, Mori D, Yano Y, Shiota M, Iwao H, Goto H, et al. Protein phosphatase 4
767 catalytic subunit regulates Cdk1 activity and microtubule organization via NDEL1
768 dephosphorylation. J Cell Biol. 2008;180: 1133–1147. doi:10.1083/jcb.200705148
769 48. Ohsugi M, Adachi K, Horai R, Kakuta S, Sudo K, Kotaki H, et al. Kid-Mediated
770 Chromosome Compaction Ensures Proper Nuclear Envelope Formation. Cell. 2008;132:
771 771–782. doi:10.1016/j.cell.2008.01.029
772 49. Kumar JP. Building an ommatidium one cell at a time. Dev Dyn. 2012;241: 136–149.
773 doi:10.1002/dvdy.23707
774 50. Nériec N, Desplan C. From the Eye to the Brain. Development of the Drosophila Visual
775 System. Curr Top Dev Biol. 2016;116: 247–271. doi:10.1016/bs.ctdb.2015.11.032
776 51. Wittmann CW, Wszolek MF, Shulman JM, Salvaterra PM, Lewis J, Hutton M, et al.
777 Tauopathy in Drosophila: Neurodegeneration without neurofibrillary tangles. Science.
778 2001;293: 711–714. doi:10.1126/science.1062382
779 52. Cukier HN, Perez AM, Collins AL, Zhou Z, Zoghbi HY, Botas J. Genetic modifiers of
780 MeCP2 function in Drosophila. Orr H, editor. PLoS Genet. 2008;4: e1000179.
781 doi:10.1371/journal.pgen.1000179
782 53. Bilen J, Bonini NM. Genome-wide screen for modifiers of ataxin-3 neurodegeneration in
783 Drosophila. PLoS Genet. 2007;3: 1950–1964. doi:10.1371/journal.pgen.0030177
784 54. Iyer J, Wang Q, Le T, Pizzo L, Grönke S, Ambegaokar SS, et al. Quantitative assessment
785 of eye phenotypes for functional genetic studies using Drosophila melanogaster. G3
786 Genes, Genomes, Genet. 2016;6: 1427–1437. doi:10.1534/g3.116.027060
787 55. Rosenberg MJ, Agarwala R, Bouffard G, Davis J, Fiermonte G, Hilliard MS, et al. Mutant
788 deoxynucleotide carrier is associated with congenital microcephaly. Nat Genet. 2002;32:
789 175–179. doi:10.1038/ng948
790 56. Chintapalli VR, Wang J, Dow JAT. Using FlyAtlas to identify better Drosophila
791 melanogaster models of human disease. Nat Genet. 2007;39: 715–720.
792 doi:10.1038/ng2049
793 57. Claes L, Del-Favero J, Ceulemans B, Lagae L, Van Broeckhoven C, De Jonghe P. De
794 novo mutations in the sodium-channel gene SCN1A cause severe myoclonic epilepsy of
795 infancy. Am J Hum Genet. 2001;68: 1327–1332. doi:10.1086/320609
796 58. Ardlie KG, DeLuca DS, Segrè A V., Sullivan TJ, Young TR, Gelfand ET, et al. The
797 Genotype-Tissue Expression (GTEx) pilot analysis: Multitissue gene regulation in
798 humans. Science. 2015;348: 648–660. doi:10.1126/science.1262110
799 59. Ernst C. Proliferation and Differentiation Deficits are a Major Convergence Point for
800 Neurodevelopmental Disorders. Trends Neurosci. 2016;39: 290–299.
801 doi:10.1016/j.tins.2016.03.001
802 60. Marchetto MC, Belinson H, Tian Y, Freitas BC, Fu C, Vadodaria KC, et al. Altered

803 proliferation and networks in neural cells derived from idiopathic autistic individuals. Mol
804 Psychiatry. 2017;22: 820–835. doi:10.1038/mp.2016.95
805 61. Wei H, Alberts I, Li X. The apoptotic perspective of autism. Int J Dev Neurosci. 2014;36:
806 13–18. doi:10.1016/j.ijdevneu.2014.04.004
807 62. Hartl TA, Scott MP. Wing tips: The wing disc as a platform for studying Hedgehog
808 signaling. Methods. 2014;68: 199–206. doi:10.1016/j.ymeth.2014.02.002
809 63. de Celis JF, García-Bellido A. Roles of the Notch gene in Drosophila wing
810 morphogenesis. Mech Dev. 1994;46: 109–122. doi:10.1016/0925-4773(94)90080-9
811 64. Raftery LA, Umulis DM. Regulation of BMP activity and range in Drosophila wing
812 development. Curr Opin Cell Biol. 2012;24: 158–65. doi:10.1016/j.ceb.2011.11.004
813 65. Diaz-Benjumea FJ, Cohen SM. Serrate signals through Notch to establish a Wingless-
814 dependent organizer at the dorsal/ventral compartment boundary of the Drosophila wing.
815 Development. 1995;121: 4215–4225.
816 66. Becam I, Milán M. A permissive role of Notch in maintaining the DV affinity boundary of
817 the Drosophila wing. Dev Biol. 2008;322: 190–8. doi:10.1016/j.ydbio.2008.07.028
818 67. Zecca M, Basler K, Struhl G. Sequential organizing activities of engrailed, hedgehog and
819 decapentaplegic in the Drosophila wing. Development. 1995;121: 2265–2278.
820 doi:10.5167/uzh-1053
821 68. Tabata T, Kornberg TB. Hedgehog is a signaling protein with a key role in patterning
822 Drosophila imaginal discs. Cell. 1994;76: 89–102. doi:10.1016/0092-8674(94)90175-9
823 69. O'Roak BJ, Vives L, Girirajan S, Karakoc E, Krumm N, Coe BP, et al. Sporadic autism
824 exomes reveal a highly interconnected protein network of de novo mutations. Nature.
825 2012;485: 246–250. doi:10.1038/nature10989
826 70. Hahn H, Wicking C, Zaphiropoulos PG, Gailani MR, Shanley S, Chidambaram A, et al.
827 Mutations of the human homolog of drosophila patched in the nevoid basal cell carcinoma
828 syndrome. Cell. 1996;85: 841–851. doi:10.1016/S0092-8674(00)81268-4
829 71. Johnson RL, Rothman AL, Xie J, Goodrich L V., Bare JW, Bonifas JM, et al. Human
830 homolog of patched, a candidate gene for the basal cell nevus syndrome. Science.
831 1996;272: 1668–1671. doi:10.1126/science.272.5268.1668
832 72. Swarup S, Pradhan-Sundd T, Verheyen EM. Genome-wide identification of phospho-
833 regulators of Wnt signaling in Drosophila. Dev. 2015;142: 1502–1515.
834 doi:10.1242/dev.116715
835 73. Six EM, Ndiaye D, Sauer G, Laâbi Y, Athman R, Cumano A, et al. The Notch ligand
836 Delta1 recruits Dlg1 at cell-cell contacts and regulates cell migration. J Biol Chem.
837 2004;279: 55818–55826. doi:10.1074/jbc.M408022200
838 74. Greene CS, Krishnan A, Wong AK, Ricciotti E, Zelaya RA, Himmelstein DS, et al.
839 Understanding multicellular function and disease with human tissue-specific networks.
840 Nat Genet. 2015;47: 569–576. doi:10.1038/ng.3259
841 75. Bult CJ, Blake JA, Smith CL, Kadin JA, Richardson JE, Mouse Genome Database Group.
842 Mouse Genome Database (MGD) 2019. Nucleic Acids Res. 2019;47: D801–D806.
843 doi:10.1093/nar/gky1056
844 76. Zhou W, Zhang L, Guoxiang X, Mojsilovic-Petrovic J, Takamaya K, Sattler R, et al.
845 GluR1 controls dendrite growth through its binding partner, SAP97. J Neurosci. 2008;28:
846 10220–10233. doi:10.1523/JNEUROSCI.3434-08.2008
847 77. Iizuka-Kogo A, Ishidao T, Akiyama T, Senda T. Abnormal development of urogenital

848 organs in Dlgh1-deficient mice. Development. 2007;134: 1799–1807.
849 doi:10.1242/dev.02830
850 78. Mahoney ZX, Sammut B, Xavier RJ, Cunningham J, Go G, Brim KL, et al. Discs-large
851 homolog 1 regulates smooth muscle orientation in the mouse ureter. Proc Natl Acad Sci U
852 S A. 2006;103: 19872–19877. doi:10.1073/pnas.0609326103
853 79. Caruana G, Bernstein A. Craniofacial dysmorphogenesis including cleft palate in mice
854 with an insertional mutation in the discs large gene. Mol Cell Biol. 2001;21: 1475–83.
855 doi:10.1128/MCB.21.5.1475-1483.2001
856 80. Chapman DL, Papaioannou VE. Three neural tubes in mouse embryos with mutations in
857 the T-box gene Tbx6. Nature. 1998;391: 695–697. doi:10.1038/35624
858 81. Ashburner M, Ball CA, Blake JA, Botstein D, Butler H, Cherry JM, et al. Gene ontology:
859 Tool for the unification of biology. Nat Genet. 2000;25: 25–29. doi:10.1038/75556
860 82. Carbon S, Douglass E, Dunn N, Good B, Harris NL, Lewis SE, et al. The Gene Ontology
861 Resource: 20 years and still GOing strong. Nucleic Acids Res. 2019;47: D330–D338.
862 doi:10.1093/nar/gky1055
863 83. Pabis M, Neufeld N, Shav-Tal Y, Neugebauer KM. Binding properties and dynamic
864 localization of an alternative isoform of the cap-binding complex subunit CBP20.
865 Nucleus. 2010;1: 412–421. doi:10.4161/nucl.1.5.12839
866 84. Di Padova M, Bruno T, De Nicola F, Iezzi S, D'Angelo C, Gallo R, et al. Che-1 arrests
867 human colon carcinoma cell proliferation by displacing HDAC1 from the p21WAF1/CIP1
868 promoter. J Biol Chem. 2003;278: 36496–504. doi:10.1074/jbc.M306694200
869 85. Bruno T, De Angelis R, De Nicola F, Barbato C, Di Padova M, Corbi N, et al. Che-1
870 affects cell growth by interfering with the recruitment of HDAC1 by Rb. Cancer Cell.
871 2002;2: 387–399. doi:10.1016/S1535-6108(02)00182-4
872 86. Page G, Lödige I, Kögel D, Scheidtmann KH. AATF, a novel transcription factor that
873 interacts with Dlk/ZIP kinase and interferes with apoptosis. FEBS Lett. 1999;462: 187–91.
874 doi:10.1016/s0014-5793(99)01529-x
875 87. Sumiyoshi E, Sugimoto A, Yamamoto M. Protein phosphatase 4 is required for
876 centrosome maturation in mitosis and sperm meiosis in C. elegans. J Cell Sci. 2002;115:
877 1403–1410.
878 88. Jensen M, Girirajan S. An interaction-based model for neuropsychiatric features of copy-
879 number variants. PLoS Genet. 2019;15: e1007879. doi:10.1371/journal.pgen.1007879
880 89. Girirajan S, Rosenfeld JA, Coe BP, Parikh S, Friedman N, Goldstein A, et al. Phenotypic
881 Heterogeneity of Genomic Disorders and Rare Copy-Number Variants. N Engl J Med.
882 2012;367: 1321–1331. doi:10.1056/NEJMoa1200395
883 90. Coe BP, Girirajan S, Eichler EE. A genetic model for neurodevelopmental disease. Curr
884 Opin Neurobiol. 2012;22: 829–836. doi:10.1016/j.conb.2012.04.007
885 91. Nicholas AK, Swanson EA, Cox JJ, Karbani G, Malik S, Springell K, et al. The molecular
886 landscape of ASPM mutations in primary microcephaly. J Med Genet. 2009;46: 249–253.
887 doi:10.1136/jmg.2008.062380
888 92. Lindsay EA, Vitelli F, Su H, Morishima M, Huynh T, Pramparo T, et al. Tbx1
889 haploinsufficiency in the DiGeorge syndrome region causes aortic arch defects in mice.
890 Nature. 2001;410: 97–101. doi:10.1038/35065105
891 93. Kishino T, Lalande M, Wagstaff J. UBE3A/E6-AP mutations cause Angelman syndrome.
892 Nat Genet. 1997;15: 70–73. doi:10.1038/ng0197-70

893 94. Brand AH, Perrimon N. Targeted gene expression as a means of altering cell fates and
894 generating dominant phenotypes. Development. 1993;118: 401–15.
895 doi:10.1101/lm.1331809
896 95. Schindelin J, Arganda-Carreras I, Frise E, Kaynig V, Longair M, Pietzsch T, et al. Fiji: An
897 open-source platform for biological-image analysis. Nat Methods. 2012;9: 676–682.
898 doi:10.1038/nmeth.2019
899 96. Kanehisa M, Sato Y, Furumichi M, Morishima K, Tanabe M. New approach for
900 understanding genome variations in KEGG. Nucleic Acids Res. 2019;47: D590–D595.
901 doi:10.1093/nar/gky962
902 97. Hagberg AA, Schult DA, Swart PJ. Exploring network structure, dynamics, and function
903 using NetworkX. 7th Python in Science Conference (SciPy 2008). 2008. pp. 11–15.
904 98. Mi H, Huang X, Muruganujan A, Tang H, Mills C, Kang D, et al. PANTHER version 11:
905 Expanded annotation data from Gene Ontology and Reactome pathways, and data analysis
906 tool enhancements. Nucleic Acids Res. 2017;45: D183–D189. doi:10.1093/nar/gkw1138
907 99. Shannon P, Markiel A, Ozier O, Baliga NS, Wang JT, Ramage D, et al. Cytoscape: A
908 software environment for integrated models of biomolecular interaction networks.
909 Genome Res. 2003;13: 2498–2504. doi:10.1101/gr.1239303
910 100. Köhler S, Carmody L, Vasilevsky N, Jacobsen JOB, Danis D, Gourdine JP, et al.
911 Expansion of the Human Phenotype Ontology (HPO) knowledge base and resources.
912 Nucleic Acids Res. 2019;47: D1018–D1027. doi:10.1093/nar/gky1105
913

914 **FIGURE LEGENDS**

915 **Figure 1. Experimental approach to identify developmental phenotypes of homologs of**
916 **CNV genes in the *Drosophila* wing.** Strategy for identifying non-neuronal phenotypes and
917 underlying cellular mechanisms for homologs of CNV and known neurodevelopmental genes
918 using the fly wing as a model system. We evaluated 59 *Drosophila* homologs of genes within 10
919 CNV regions and 20 known neurodevelopmental genes (79 total homologs). Using the *UAS-*
920 *GAL4* system with wing-specific bx^{MS1096} driver, we knocked down 136 individual RNAi lines
921 for homologs of CNV and neurodevelopmental genes, and evaluated qualitative and quantitative
922 phenotypes. We next clustered RNAi lines based on severity of qualitative phenotypes, and
923 compared adult wing phenotypes to phenotypes observed with ubiquitous and eye-specific
924 knockdown of homologs. Furthermore, we evaluated underlying cellular mechanisms for the
925 observed wing-specific phenotypes, and examined the connectivity patterns of candidate
926 homologs for developmental phenotypes in multiple human tissue-specific gene networks.
927

928 **Figure 2. Global analysis of developmental phenotypes with knockdown of homologs of**
929 **CNV genes. (A)** Representative brightfield images of adult wing phenotype severity observed
930 with knockdown of homologs of CNV genes, based on clustering analysis, are shown. **(B)**
931 Heatmap with k-means clustering of qualitative phenotypes in adult female wings across 136
932 RNAi lines is shown. The color of each cell represents the frequency of individual fly wings
933 (n=20-25 adult wings) for each RNAi line (x-axis) that show a specific severity (no phenotype,
934 mild, moderate, severe, lethal) for the five qualitative phenotypes assessed (y-axis; wrinkled
935 wings, ectopic veins, missing veins, discoloration, bristle planar polarity), as detailed in **S3 Data**.
936 Based on these data, we identified clusters for no phenotype (n=75 lines), mild (n=24 lines),

937 moderate (n=10 lines), severe (n=21 lines), and lethal (n=6 lines) RNAi lines. **(C)** Summary
938 table of qualitative and quantitative adult wing phenotypes for all tested RNAi lines of homologs
939 of CNV and neurodevelopmental genes. Quantitative phenotype totals do not include lethal
940 RNAi lines for both area and vein length. In addition, L3 vein length totals do not include severe
941 RNAi lines.
942
943 **Figure 3. Qualitative adult wing phenotypes of *Drosophila* homologs of CNV and**
944 **neurodevelopmental genes.** Heatmaps representing five qualitative adult wing phenotypes for
945 all 136 RNAi lines, with **(A)** 59 tested homologs for 10 CNV regions and **(B)** 20 homologs for
946 neurodevelopmental genes (β-catenin, core neurodevelopmental genes, and microcephaly genes),
947 are shown. The color of each cell represents the frequency of each qualitative phenotype by
948 severity (wrinkled wings, WR; ectopic veins, EV; missing veins, MV; discoloration, DC; bristle
949 planar polarity, BP), ranging from no phenotype to lethal. **(C)** Representative brightfield images
950 of adult fly wings (scale bar = 500μm) with wing-specific knockdown of homologs of CNV and
951 neurodevelopmental genes showing the five assessed qualitative phenotypes, including
952 discoloration, wrinkled wings, bristle polarity, ectopic veins, and missing veins, are shown.
953 Panels in the *bx*^{MS1096}*-GAL4* control and *C6836*^{KK112485} images highlight bristle planar polarity
954 phenotypes for the representative images. Black arrowheads highlight ectopic veins, and white
955 arrowheads highlight missing veins. Genotypes for the images are: *w*^{1118}*/bx*^{MS1096}*-GAL4;+; UAS-*
956 *Dicer2/+*, *w*^{1118}*/bx*^{MS1096}*-GAL4;UAS-Rph*^{GD7330} *RNAi/+;UAS-Dicer2/+*, *w*^{1118}*/bx*^{MS1096}*-*
957 *GAL4;UAS-CG15528*^{KK107736} *RNAi/+; UAS-Dicer2/+*, *w*^{1118}*/bx*^{MS1096}*-GAL4;UAS-CG6836*^{KK112485}
958 *RNAi/+; UAS-Dicer2/+*, *w*^{1118}*/bx*^{MS1096}*-GAL4;+;UAS-CG14182*^{GD2738} *RNAi/UAS-Dicer2*, and
959 *w*^{1118}*/bx*^{MS1096}*-GAL4;UAS-kis*^{KK100890} *RNAi/+; UAS-Dicer2/+*.

960

961 **Figure 4. Quantitative adult wing phenotypes of *Drosophila* homologs of CNV and**
962 **neurodevelopmental genes. (A)** Representative brightfield images of adult fly wings (scale bar
963 = 500μm) with wing-specific knockdown of homologs of CNV and neurodevelopmental genes
964 with size defects are shown. The bx^{MS1096}-*GAL4* control image highlights six veins, including
965 longitudinal veins L2, L3, L4, and L5 as well as the anterior and posterior crossveins (ACV and
966 PCV), that were measured for quantitative analysis. The dotted line in the control image
967 represents the total wing area calculated for each RNAi line. Genotypes for the images are:
968 w^{1118}/bx^{MS1096}-*GAL4;+; UAS-Dicer2/+*, w^{1118}/bx^{MS1096}-*GAL4;UAS-Fmo-2*^{KK109203} *RNAi/+; UAS-*
969 *Dicer2/+*, and w^{1118}/bx^{MS1096}-*GAL4;+;UAS-Trpm*^{GD4541} *RNAi/UAS-Dicer2*. **(B)** Boxplot of L3
970 vein lengths for knockdown of select homologs in adult fly wings (n = 9-91, *$p < 0.05$, two-
971 tailed Mann–Whitney test with Benjamini-Hochberg correction). Vein measurements for all
972 other longitudinal veins and crossveins (ACV and PCV) for these lines are represented in **S3 Fig**.
973 **(C)** Boxplot of wing areas for knockdown of select homologs in adult fly wings (n = 9-91,
974 *$p < 0.05$, two-tailed Mann–Whitney test with Benjamini-Hochberg correction). Boxplots
975 indicate median (center line), 25th and 75th percentiles (bounds of box), and minimum and
976 maximum (whiskers), with red dotted lines representing the control median.

977

978 **Figure 5. Comparison of wing-specific, eye-specific, and ubiquitous knockdown of fly**
979 **homologs. (A)** Heatmap with the penetrance of phenotypes with ubiquitous knockdown (*da–*
980 *GAL4*) of select homologs of CNV genes, compared to their adult wing-specific (bx^{MS1096}–*GAL4*)
981 phenotypic severity, is shown. **(B)** Boxplots of *Flynotyper*-derived phenotypic scores for adult
982 eyes with eye-specific knockdown (*GMR-GAL4*) of select fly homologs, normalized as fold-

983 change (FC) to control values (n = 7–40, *p < 0.05, one-tailed Mann–Whitney test with
984 Benjamini-Hochberg correction). Boxplots are arranged by severity of adult wing phenotypes,
985 while eye phenotypic scores are categorized by severity: no change (0–1.1 FC), mild (1.1–1.5
986 FC), moderate (1.5–2.0 FC), and severe (>2.0 FC). **(C)** Boxplot showing average eye phenotypic
987 scores for 66 RNAi lines of select fly homologs, normalized as fold-change (FC) to control
988 values, according to wing phenotypic category (n=4–30 RNAi lines per group). We did not
989 observe significant changes in eye phenotype severity across the five wing phenotypic categories
990 (Kruskal-Wallis rank sum test, p=0.567, df = 5, $\chi^2 = 3.881$). Examples of average eye phenotypic
991 scores for RNAi lines with no phenotype (*para*^{GD3392_1}), mild (*rl*^{KK115768}), and lethal (*dlg1*^{GD4689})
992 wing phenotypes are highlighted in the plot. Boxplots indicate median (center line), 25th and
993 75th percentiles (bounds of box), and minimum and maximum (whiskers), with red dotted lines
994 representing the control median. **(D)** Representative brightfield adult eye (scale bar = 100 µm)
995 and wing (scale bar = 500µm) images with tissue-specific knockdown of CNV homologs are
996 shown. Genotypes for the eye images are: *w*^{1118}*;GMR-GAL4/+; UAS-Dicer2/+, w*^{1118}*;GMR-*
997 *GAL4/UAS-Lnk*^{KK105731} *RNAi; UAS-Dicer2/+*, *w*^{1118}*;GMR-GAL4/UAS-mEFTu1*^{GD16961} *RNAi;*
998 *UAS-Dicer2/+*. Genotypes for the wing images are: *w*^{1118}*/bx*^{MS1096}*-GAL4;+; UAS-Dicer2/+*,
999 *w*^{1118}*/bx*^{MS1096}*-GAL4; UAS-Lnk*^{KK105731} *RNAi/+; UAS-Dicer2/+*, and *w*^{1118}*/bx*^{MS1096}*-GAL4; UAS-*
1000 *mEFTu1*^{GD16961} *RNAi/+; UAS-Dicer2/+*.
1001
1002 **Figure 6. Expression patterns of *Drosophila* homologs and human CNV and**
1003 **neurodevelopmental genes across multiple tissues. (A)** Heatmap with expression of fly
1004 homologs of select CNV and neurodevelopmental genes in multiple *Drosophila* larval and adult
1005 tissues (derived from the FlyAtlas Anatomical Microarray dataset), compared with adult wing

1006 phenotype severity, is shown. Expression values are grouped into no expression (<10 fragments
1007 per kilobase of transcript per million reads, or FPKM), low (10–100 FPKM), moderate (100–500
1008 FPKM), high (500–1000 FPKM), and very high (>1000 FPKM) expression categories. **(B)**
1009 Heatmap with expression of select human CNV and neurodevelopmental genes in multiple adult
1010 tissues, derived from the Genotype-Tissue Expression (GTEx) dataset v.1.2, is shown.
1011 Expression values are grouped into no expression (<3 transcripts per million reads, or TPM), low
1012 (3–10 TPM), moderate (10–25 TPM), high (25–100 TPM), and very high (>100 TPM)
1013 expression categories. "X" symbols denote preferential expression in a particular tissue (see
1014 **Methods**). Expression data for all CNV and neurodevelopmental genes are provided in **S7 Data**.
1015

1016 **Figure 7. *Drosophila* homologs of CNV and neurodevelopmental genes show altered levels**
1017 **of apoptosis and proliferation. (A)** Larval imaginal wing discs (scale bar = 50 μm) stained with
1018 nuclear marker DAPI, apoptosis marker dcp1, and cell proliferation marker pH3 illustrate altered
1019 levels of apoptosis and cell proliferation due to wing-specific knockdown of select fly homologs
1020 of CNV genes. We quantified the number of stained cells within the wing pouch of the wing disc
1021 (white box), which becomes the adult wing. Additional representative images of select homologs
1022 are presented in **S6 Fig**. Genotypes for the wing images are: w^{1118}/bx^{MS1096}*-GAL4;+; UAS-*
1023 *Dicer2/+*, w^{1118}/bx^{MS1096}*-GAL4;+; UAS-Aatf*^{GD7229} *RNAi/UAS-Dicer2*, w^{1118}/bx^{MS1096}*-GAL4;UAS-*
1024 *Pp4-19C*^{GD9561}*/+; UAS-Dicer2/+,* w^{1118}/bx^{MS1096}*-GAL4;+; UAS-Atx2*^{GD11562} *RNAi/UAS-Dicer2*,
1025 and w^{1118}/bx^{MS1096}*-GAL4;+; UAS-Sin*^{GD7027} *RNAi/UAS-Dicer2.* **(B)** Box plot of dcp1-positive
1026 cells in larval wing discs with knockdown of select fly homologs of CNV and
1027 neurodevelopmental genes, normalized to controls (n = 7–18, *p < 0.05, two-tailed Mann–
1028 Whitney test with Benjamini-Hochberg correction). We note that several RNAi lines showed

1029 severe dcp1 staining across the entire wing disc and could not be quantified. The number of dcp1
1030 positive cells were calculated manually. **(C)** Box plot of pH3-positive cells in the larval wing
1031 discs with knockdown of select fly homologs of CNV and neurodevelopmental genes,
1032 normalized to controls ($n = 6–18$, $*p < 0.05$, two-tailed Mann–Whitney test with Benjamini-
1033 Hochberg correction). The number of pH3 positive cells were calculated using the
1034 AnalyzeParticles function in ImageJ. Boxplots are organized by adult wing phenotype (wing size
1035 defect, mild, moderate (mod.), severe (sev.), lethal). Boxplots indicate median (center line), 25th
1036 and 75th percentiles (bounds of box), and minimum and maximum (whiskers), with red dotted
1037 lines representing the control median.
1038
1039 **Figure 8. Candidate *Drosophila* homologs of genes within CNV regions interact with**
1040 **conserved signaling pathways.** Larval imaginal wing discs (scale bar = 50 μm) stained with **(A)**
1041 wingless, **(B)** patched, **(C)** engrailed, and **(D)** delta illustrate disrupted expression patterns for
1042 proteins located within the Wnt (wingless), Hedgehog (patched and engrailed), and Notch (delta)
1043 signaling pathways due to wing-specific knockdown of select fly homologs. Dotted yellow boxes
1044 represent expression patterns for signaling proteins in *bx*^{MS1096}*-GAL4* control images. White
1045 arrowheads and dotted white boxes highlight disruptions in expression patterns of signaling
1046 proteins with knockdown of homologs of CNV or neurodevelopmental genes. Additional
1047 representative images of select homologs are presented in **S8 Fig**. Genotypes for the wing
1048 images are: *w*^{1118}*/bx*^{MS1096}*-GAL4;+; UAS-Dicer2/+*, *w*^{1118}*/bx*^{MS1096}*-GAL4;UAS-Pp4-19C*^{GD9561}*/+;*
1049 *UAS-Dicer2/+, w*^{1118}*/bx*^{MS1096}*-GAL4;UAS-Cbp20*^{KK109448}*/+; UAS-Dicer2/+*, *w*^{1118}*/bx*^{MS1096}*-*
1050 *GAL4;+; UAS-Sin*^{GD7027} *RNAi/UAS-Dicer2, w*^{1118}*/bx*^{MS1096}*-GAL4;+; UAS-Aatf*^{GD7229} *RNAi/UAS-*
1051 *Dicer2*, and *w*^{1118}*/bx*^{MS1096}*-GAL4;UAS-Klp61F*^{GD14149}*/+; UAS-Dicer2/+*.

1052

1053 **Figure 9. Connectivity of human CNV genes with conserved signaling pathway genes in**
1054 **human tissue-specific networks. (A)** Diagrams representing the connectivity of eight human
1055 CNV and neurodevelopmental genes whose fly homologs disrupt the Notch signaling pathway to
1056 57 human Notch signaling genes within kidney, heart, and brain-specific gene interaction
1057 networks are shown. Yellow nodes represent CNV and neurodevelopmental genes, pink nodes
1058 represent Notch signaling pathway genes, and green nodes represent connector genes located
1059 within the shortest paths between CNV and Notch pathway genes. **(B)** Violin plots showing the
1060 average connectivity (i.e. inverse of shortest path lengths) of human CNV genes to genes in
1061 Hedgehog, Notch, and Wnt signaling pathways across three tissue-specific networks (n=322–810
1062 pairs of genes, *$p < 0.05$, two-tailed Welch's t-test with Benjamini-Hochberg correction). **(C)**
1063 Table showing clusters of enriched Gene Ontology (GO) Biological Process terms for connector
1064 genes observed for each signaling pathway in the three tested tissue-specific networks,
1065 categorized by enrichments in ubiquitous, neuronal, and non-neuronal tissues ($p<0.05$, Fisher's
1066 Exact test with Benjamini-Hochberg correction).

1067

1068 **Figure 10. Multiple genes contribute towards neuronal and non-neuronal phenotypes**
1069 **associated with pathogenic CNVs.** While a subset of genes within CNV regions contribute
1070 towards tissue-specific phenotypes, a majority of genes contribute towards both neuronal and
1071 non-neuronal phenotypes through disruption of developmental signaling pathways and global
1072 biological processes.

1073 **SUPPORTING INFORMATION LEGENDS**

1074 **S1 Figure. Phenotypic expression of CNV carriers across tissues.** Heatmap with frequencies
1075 of non-neuronal developmental phenotypes observed in 1,225 human carriers of 10 pathogenic
1076 CNV deletions, curated from the DECIPHER database, is shown. CNV carriers show a variety of
1077 phenotypes that manifest across different tissues, including eye, limbs, muscle, and skeleton.

1078

1079 **S2 Figure. Quantitative vein length phenotypes for select *Drosophila* homologs of CNV and**
1080 **neurodevelopmental genes.** Boxplots of **(A)** L2, **(B)** L4, and **(C)** L5, longitudinal veins, and **(D)**
1081 anterior crossvein (ACV) and **(E)** posterior crossvein (PCV) lengths for knockdown of select
1082 homologs in adult fly wings ($n = 9\text{-}91$, $*p < 0.05$, two-tailed Mann–Whitney test with Benjamini-
1083 Hochberg correction). Boxplots indicate median (center line), 25th and 75th percentiles (bounds
1084 of box), and minimum and maximum (whiskers), with red dotted lines representing the control
1085 median.

1086

1087 **S3 Figure. Comparisons of eye-specific and wing-specific knockdowns for select *Drosophila***
1088 **homologs of CNV and neurodevelopmental genes.** Boxplots of *Flynotyper*-derived phenotypic
1089 scores for 66 tested adult eyes with eye-specific knockdown (*GMR-GAL4*) of select homologs of
1090 CNV and neurodevelopmental genes, normalized as fold-change (FC) to control values ($n = 1$–
1091 40, $*p < 0.05$, one-tailed Mann–Whitney test with Benjamini-Hochberg correction). RNAi lines
1092 that do not show any observable qualitative adult wing phenotypes, including lines that show
1093 wing measurement phenotypes, are represented in **(A)**, while RNAi lines with observable mild to
1094 lethal qualitative wing phenotypes are represented in **(B)**. Boxplots indicate median (center line),

1095 25th and 75th percentiles (bounds of box), and minimum and maximum (whiskers), with red
1096 dotted lines representing the control median.
1097
1098 **S4 Figure. Expression of *Drosophila* homologs of CNV and neurodevelopmental genes in**
1099 **larval and adult tissues.** Venn diagrams representing the number of 76/77 fly homologs of
1100 CNV and neurodevelopmental genes that are expressed (>10 fragments per kilobase of transcript
1101 per million reads, or FPKM) in **(A)** larval (central nervous system or CNS, gut, trachea, and fat
1102 body) and **(B)** adult tissues (brain, gut, heart and fat body) are shown.
1103
1104 **S5 Figure. Additional *Drosophila* homologs of CNV and neurodevelopmental genes show**
1105 **altered levels of cell proliferation and apoptosis.** Larval imaginal wing discs (scale
1106 bar = 50 μm) stained with nuclear marker DAPI, apoptosis marker dcp1, and cell proliferation
1107 marker pH3 illustrate altered levels of cell proliferation and apoptosis due to wing-specific
1108 knockdown of select fly homologs of CNV genes. We examined changes in the number of
1109 stained cells within the wing pouch of the wing disc (white box), which becomes the adult wing.
1110 Genotypes for the wing images are: w^{1118}/bx^{MS1096}-*GAL4;+; UAS-Dicer2/+*, w^{1118}/bx^{MS1096}-
1111 *GAL4;UAS-Cbp20*^{KK109448}*/+; UAS-Dicer2/+*, w^{1118}/bx^{MS1096}-*GAL4;+; UAS-dlg1*^{GD4689}
1112 *RNAi/UAS-Dicer2*, w^{1118}/bx^{MS1096}-*GAL4;UAS-CG8888*^{GD3777}*/+; UAS-Dicer2/+*, w^{1118}/bx^{MS1096}-
1113 *GAL4;+; UAS-UQCR-C2*^{GD11238} *RNAi/UAS-Dicer2*, w^{1118}/bx^{MS1096}-*GAL4;+; UAS-ACC*^{GD3482}
1114 *RNAi/UAS-Dicer2*, w^{1118}/bx^{MS1096}-*GAL4;UAS-Klp61F*^{GD14149}*/+; UAS-Dicer2/+*, and
1115 w^{1118}/bx^{MS1096}-*GAL4;UAS-Rph*^{GD7330} *RNAi/+;UAS-Dicer2/+*.
1116

1117 **S6 Figure. Select female and male *Drosophila* homologs of CNV and neurodevelopmental**
1118 **genes show altered levels of cell proliferation and apoptosis. (A)** Larval imaginal wing discs
1119 (scale bar = 50 μm) stained with nuclear marker DAPI, apoptosis marker dcp1, and cell
1120 proliferation marker pH3 illustrate altered levels of cell proliferation and apoptosis due to wing-
1121 specific knockdown of select fly homologs of CNV genes in females and males. We examined
1122 changes in the number of stained cells within the wing pouch of the wing disc (white box), which
1123 becomes the adult wing. Genotypes for the wing images are: w^{1118}*/bx*^{MS1096}*-GAL4;+; UAS-*
1124 *Dicer2/+*, w^{1118}*/bx*^{MS1096}*-GAL4;+; UAS-lgs*^{GD1241}*/UAS-Dicer2*, w^{1118}*/bx*^{MS1096}*-GAL4;+; UAS-Sra-*
1125 *1*^{GD11477}*/UAS-Dicer2*, and w^{1118}*/bx*^{MS1096}*-GAL4;UAS-CG11035*^{KK101201} *RNAi+; UAS-Dicer2/+*.
1126 **(B)** Box plot of dcp1-positive cells in larval wing discs with knockdown of select fly homologs
1127 of CNV and neurodevelopmental genes, normalized to controls ($n = 9–13$, $*p < 0.05$, two-tailed
1128 Mann–Whitney test with Benjamini-Hochberg correction). The number of dcp1 positive cells
1129 were calculated manually. **(C)** Box plot of pH3-positive cells in the larval wing discs with
1130 knockdown of select fly homologs of CNV and neurodevelopmental genes, normalized to
1131 controls ($n = 9–13$, $*p < 0.05$, two-tailed Mann–Whitney test with Benjamini-Hochberg
1132 correction). The number of pH3 positive cells were calculated using the AnalyzeParticles
1133 function in ImageJ. Boxplots indicate median (center line), 25th and 75th percentiles (bounds of
1134 box), and minimum and maximum (whiskers), with red dotted lines representing the control
1135 median.
1136
1137 **S7 Figure. Additional *Drosophila* homologs of genes within CNV regions interact with**
1138 **conserved signaling pathways to induce developmental phenotypes.** Larval imaginal wing
1139 discs (scale bar = 50 μm) stained with **(A)** wingless, **(B)** patched, **(C)** engrailed, and **(D)** delta

1140 illustrate disrupted expression patterns for proteins located within the Wnt (wingless), Hedgehog
1141 (patched and engrailed), and Notch (delta) signaling pathways due to wing-specific knockdown
1142 of additional fly homologs of CNV and neurodevelopmental genes. Dotted yellow boxes
1143 represent expression patterns for signaling proteins in *bx*^{MS1096}*-GAL4* control images. White
1144 arrowheads and dotted white boxes highlight disruptions in expression patterns of signaling
1145 proteins with knockdown of CNV or neurodevelopmental genes. Genotypes for the wing images
1146 are: *w*^{1118}*/bx*^{MS1096}*-GAL4;+; UAS-Dicer2/+*, *w*^{1118}*/bx*^{MS1096}*-GAL4;+; UAS-dlg1*^{GD4689} *RNAi/UAS-*
1147 *Dicer2*, *w*^{1118}*/bx*^{MS1096}*-GAL4;+; UAS-Tsf2*^{GD2442} *RNAi/UAS-Dicer2*, *w*^{1118}*/bx*^{MS1096}*-GAL4;+;*
1148 *UAS-Atx2*^{GD11562} *RNAi/UAS-Dicer2*, *w*^{1118}*/bx*^{MS1096}*-GAL4;+; UAS-UQCR-C2*^{GD11238} *RNAi/UAS-*
1149 *Dicer2*, *w*^{1118}*/bx*^{MS1096}*-GAL4;+; UAS-nudE*^{GD15226} *RNAi/UAS-Dicer2*, and *w*^{1118}*/bx*^{MS1096}*-*
1150 *GAL4;+; UAS-ACC*^{GD3482} *RNAi/UAS-Dicer2*.
1151
1152 **S8 Figure. Tissue-specific network diagrams showing connectivity of human CNV genes**
1153 **with conserved signaling pathway genes.** Representative diagrams for connectivity between
1154 nine human CNV and neurodevelopmental genes whose fly homologs disrupt the **(A)** Wnt and
1155 **(B)** Hedgehog signaling pathways and 162 human Wnt and 46 human Hedgehog signaling genes
1156 within kidney, heart, and brain-specific gene interaction networks are shown. Yellow nodes
1157 represent CNV and neurodevelopmental genes, pink nodes represent Notch signaling pathway
1158 genes, and green nodes represent connector genes within the shortest paths between CNV and
1159 Notch pathway genes.
1160
1161 **S1 Data (Excel file).** Non-neuronal phenotypes of individuals carrying rare pathogenic CNVs in
1162 the DECIPHER database.

1163

1164 **S2 Data (Excel file).** *Drosophila* homologs of human CNV and neurodevelopmental genes, as
1165 determined using DIOPT v.7.1. Grey shading indicates human CNV genes that were not assessed
1166 in this study.

1167

1168 **S3 Data (Excel file).** Qualitative and quantitative adult wing phenotypes for *Drosophila*
1169 homologs of human CNV and neurodevelopmental genes. This file shows the raw frequencies of
1170 severity categories for five qualitative wing phenotypes and average areas and vein lengths for
1171 all 136 female and male tested RNAi lines. The file also includes k-means clusters for the female
1172 RNAi lines.

1173

1174 **S4 Data (Excel file).** Summary of adult wing qualitative and quantitative phenotypes for tested
1175 *Drosophila* homologs. This file summarizes qualitative k-means clustering and longitudinal L3
1176 vein length and wing area changes for 79 tested fly homologs. We defined discordant homologs
1177 when multiple RNAi lines for the same fly homolog showed no phenotype versus any qualitative
1178 or quantitative phenotypes, followed by discordance for small or large quantitative phenotypes.

1179

1180 **S5 Data (Excel file).** Phenotypes of mouse knockdown models for homologs of CNV genes.
1181 This file lists lethality and neuronal and non-neuronal phenotypes, categorized using top-level
1182 Mammalian Phenotype Ontology terms, for knockdown models of 130 mouse homologs of CNV
1183 genes, derived from the Mouse Genome Informatics (MGI) database.

1184

1185 **S6 Data (Excel file).** Summary of eye-specific and wing-specific phenotypes for fly homologs.
1186 This file summarizes eye-specific and wing-specific phenotypes by severity category for fly
1187 homologs of CNV and neurodevelopmental genes. Eye phenotype severity is defined by
1188 *Flynotyper* phenotypic scores with fold-change (FC) normalization to control as follows: no
1189 change (0–1.1 FC), mild (1.1–1.5 FC), moderate (1.5–2.0 FC), and severe (>2.0 FC). Wing
1190 phenotype severity is defined by k-means clustering for qualitative phenotypes and quantitative
1191 size changes as listed in **S4 Data**.
1192
1193 **S7 Data (Excel file).** Tissue-specific expression of *Drosophila* homologs and human CNV and
1194 neurodevelopmental genes. This file lists expression values across multiple fly and human
1195 tissues for 79 *Drosophila* homologs and 150 human genes. Fly expression data (fragments per
1196 kilobase of transcript per million reads, or FPKM) was derived from the FlyAtlas Anatomical
1197 Microarray dataset, and human expression data (transcripts per million reads, or TPM) was
1198 derived from the Genotype-Tissue Expression (GTEx) dataset v.1.2.
1199
1200 **S8 Data (Excel file).** Summary of immunostaining of the larval imaginal wing discs. This file
1201 summarizes changes in apoptosis (27 homologs), cell proliferation (27 homologs), and Wnt,
1202 Hedgehog, and Notch signaling pathway proteins (14 homologs), along with qualitative and
1203 quantitative adult wing phenotypes (as listed in **S3 Data**), for female and male fly homologs.
1204
1205 **S9 Data (Excel file).** Tissue-specific network connectivity for candidate CNV genes and
1206 signaling pathway genes. This file lists the shortest path lengths between nine candidate CNV
1207 genes and 265 genes within Wnt, Hedgehog, and Notch signaling pathways for heart, kidney,

1208 and brain-specific gene interaction networks, along with the connector genes that are within the
1209 shortest paths. Enriched Gene Ontology (GO) Biological Process, Cellular Component, and
1210 Molecular Function terms for sets of connector genes for each signaling pathway in each tissue-
1211 specific networks are also provided.
1212
1213 **S10 Data (Excel file)**. List of *Drosophila* stocks used for experiments, including stock numbers
1214 and genotypes.
1215
1216 **S11 Data (Excel file).** Statistics for all experimental data. This file shows all statistical
1217 information (sample size, mean/median/standard deviation of datasets, test statistics, p-values,
1218 degrees of freedom, confidence intervals, and Benjamini-Hochberg FDR corrections) for all data.
1219 Statistical information for Kruskal-Wallis test includes factors, degrees of freedom, test statistics,
1220 and post-hoc pairwise Wilcoxon tests with Benjamini-Hochberg correction.

Figure 1

Experimental strategy

Wing-specific driver *bx^{MS1096}-GAL4* × ***UAS-RNAi*** (79 genes)

Phenotyping of adult wings

Qualitative analysis
- Wrinkled wings
- Ectopic veins
- Missing veins
- Discoloration
- Bristle planar polarity

Quantitative analysis
- Longitudinal veins (L2, L3, L4, L5)
- Crossveins (ACV, PCV)
- Wing area

Tissue-specific effects

- Compare to ubiquitous knockdown
- Compare to eye-specific knockdown
- Gene expression across multiple tissues (human and flies)

Cellular processes and developmental pathways

- Cell proliferation
- Apoptosis
- Disruptions in signaling pathways
- Human tissue-specific network analysis (brain, heart, kidney)

Figure 2

A

Phenotypic analysis of adult wings in *Drosophila*

B

K-means clustering of qualitative wing data

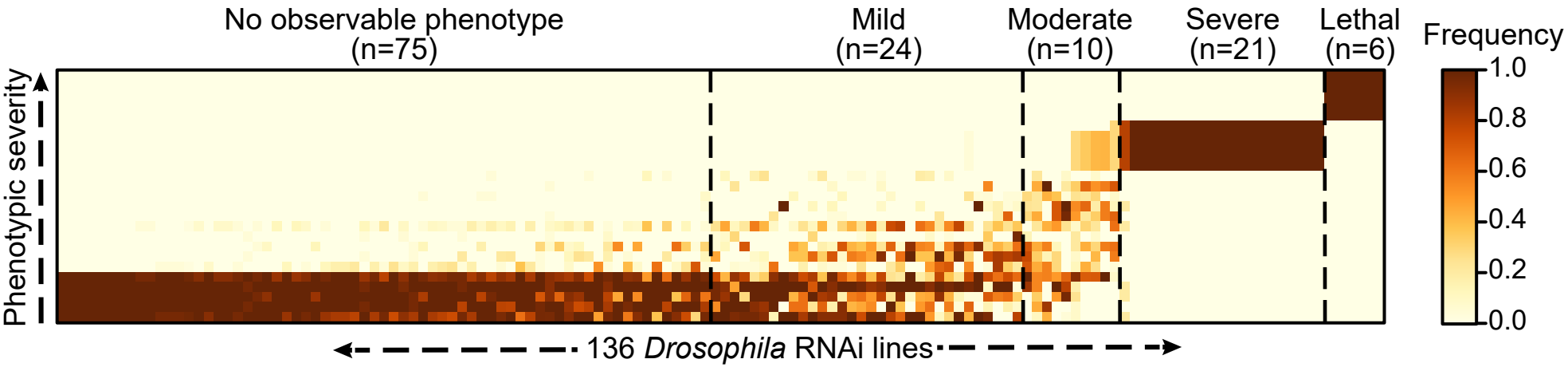

C

Summary of qualitative and quantitative adult wing phenotypes

Fly homologs	RNAi lines	Qualitative phenotypes					Quantitative phenotypes	
		No pheno.	Mild	Moderate	Severe	Lethal	Wing area	L3 vein length
CNV genes	95	45	21	7	16	6	65	53
Neurodevelopmental genes	41	30	3	3	5	0	24	21
Total	136	75	24	10	21	6	89	74

Figure 3

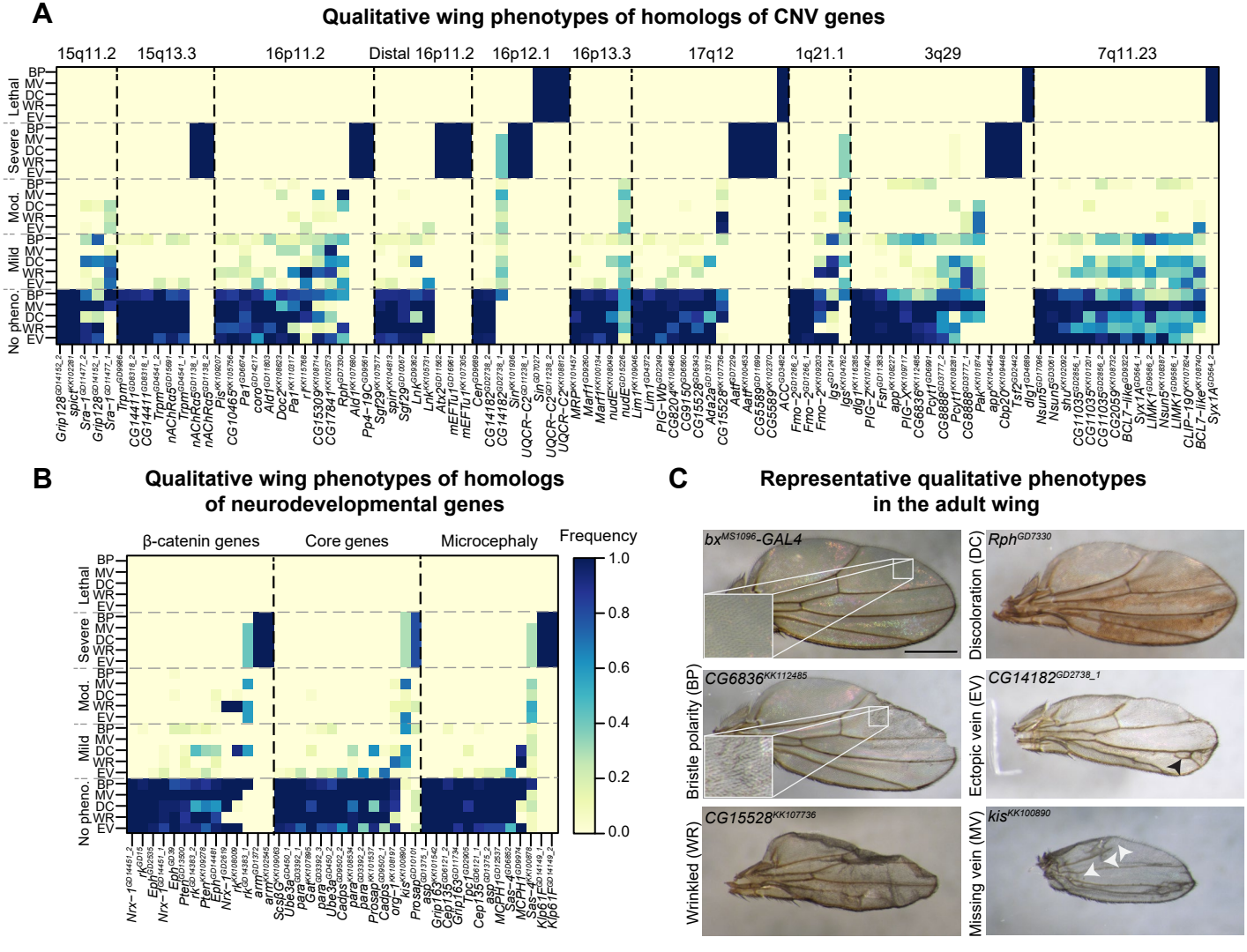
A
Qualitative wing phenotypes of homologs of CNV genes
15q11.2
15q13.3
16p11.2
Distal 16p11.2
16p12.1
16p13.3
17q12
1q21.1
3q29
7q11.23
Lethal
Severe
Mod.
Mild
No pheno.
BP
MV
DC
WR
EV
B
Qualitative wing phenotypes of homologs of neurodevelopmental genes
β-catenin genes
Core genes
Microcephaly
Frequency
1.0
0.8
0.6
0.4
0.2
0.0
C
Representative qualitative phenotypes in the adult wing
bxMS1096-GAL4
Rph GD7330
Discoloration (DC)
CG6836 KK112485
Bristle polarity (BP)
CG14182 GD2738_1
Ectopic vein (EV)
CG15528 KK107736
Wrinkled (WR)
kis KK100890
Missing vein (MV)

Figure 4

A

Representative quantitative phenotypes in the adult wing

B

L3 vein length for select homologs

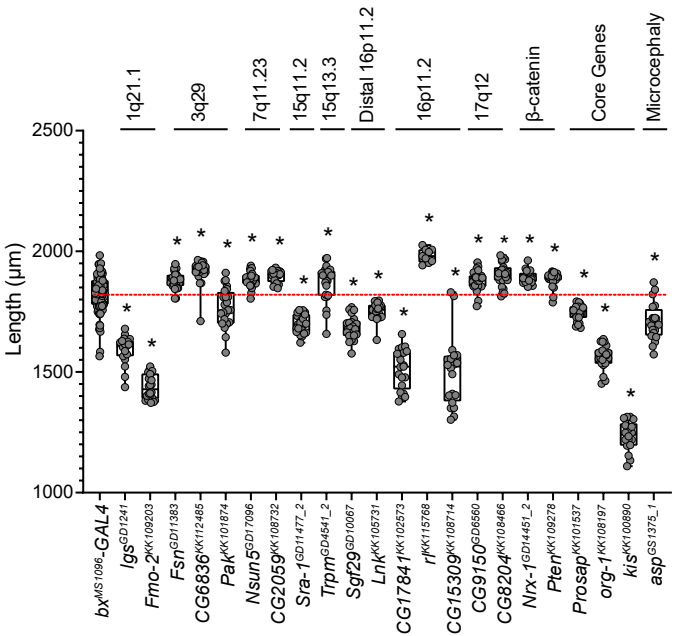

C

Wing area for select homologs

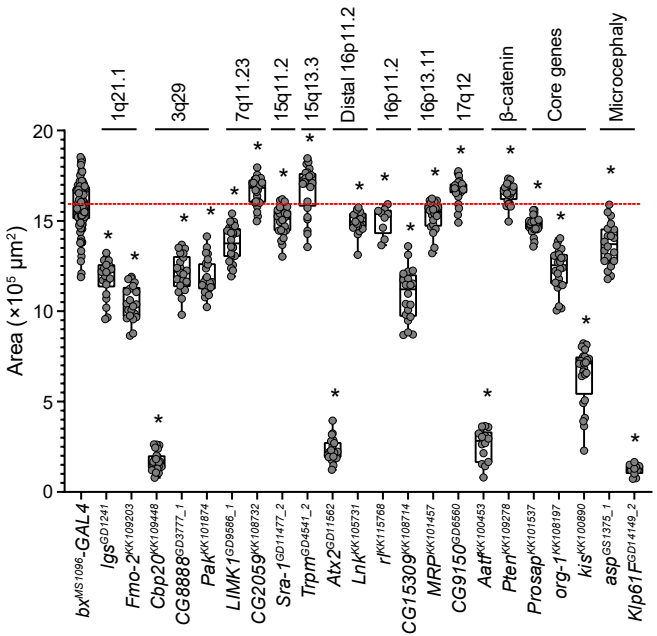

Figure 5

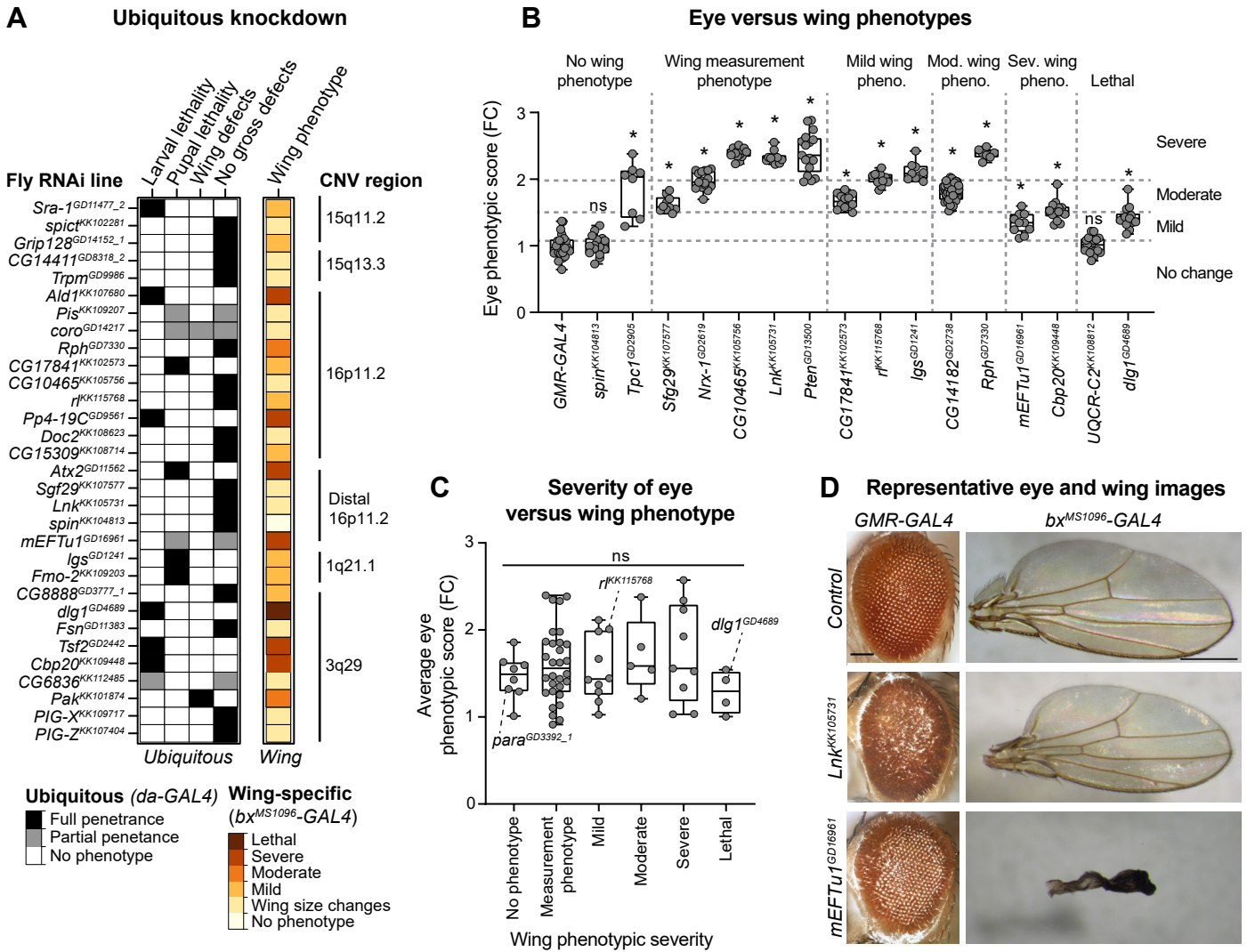
A
Ubiquitous knockdown
Larval lethality
Pupal lethality
Wing defects
No gross defects
Wing phenotype
Fly RNAi line
CNV region
Sra-1GD11477_2
spictKK102281
Grip128GD14152_1
CG14411GD8318_2
TrpmGD9986
Ald1KK107680
PisKK109207
coroGD14217
RphGD7330
CG17841KK102573
CG10465KK105756
rlKK115768
Pp4-19CGD9561
Doc2KK108623
CG15309KK108714
Atx2GD11562
Sgf29KK107577
LnkKK105731
spinKK104813
mEFTu1GD16961
IgsGD1241
Fmo-2KK109203
CG8888GD3777_1
dlg1GD4689
FsnGD11383
Tsf2GD2442
Cbp20KK109448
CG6836KK112485
PakKK101874
PIG-XKK109717
PIG-ZKK107404
15q11.2
15q13.3
16p11.2
Distal 16p11.2
1q21.1
3q29
Ubiquitous
Wing
Ubiquitous (da-GAL4)
Full penetrance
Partial penetance
No phenotype
Wing-specific (bxMS1096-GAL4)
Lethal
Severe
Moderate
Mild
Wing size changes
No phenotype
B
Eye versus wing phenotypes
No wing phenotype
Wing measurement phenotype
Mild wing pheno.
Mod. wing pheno.
Sev. wing pheno.
Lethal
Eye phenotypic score (FC)
Severe
Moderate
Mild
No change
ns
GMR-GAL4
spinKK104813
Tpc1GD2905
Sfg29KK107577
Nrx-1GD2619
CG10465KK105756
LnkKK105731
PtenGD13500
CG17841KK102573
rlKK115768
IgsGD1241
CG14182GD2738
RphGD7330
mEFTu1GD16961
Cbp20KK109448
UQCR-C2KK108812
dlg1GD4689
C
Severity of eye versus wing phenotype
Average eye phenotypic score (FC)
ns
rlKK115768
dlg1GD4689
paraGD3392_1
No phenotype
Measurement phenotype
Mild
Moderate
Severe
Lethal
Wing phenotypic severity
D
Representative eye and wing images
GMR-GAL4
bxMS1096-GAL4
Control
LnkKK105731
mEFTu1GD16961

Figure 6

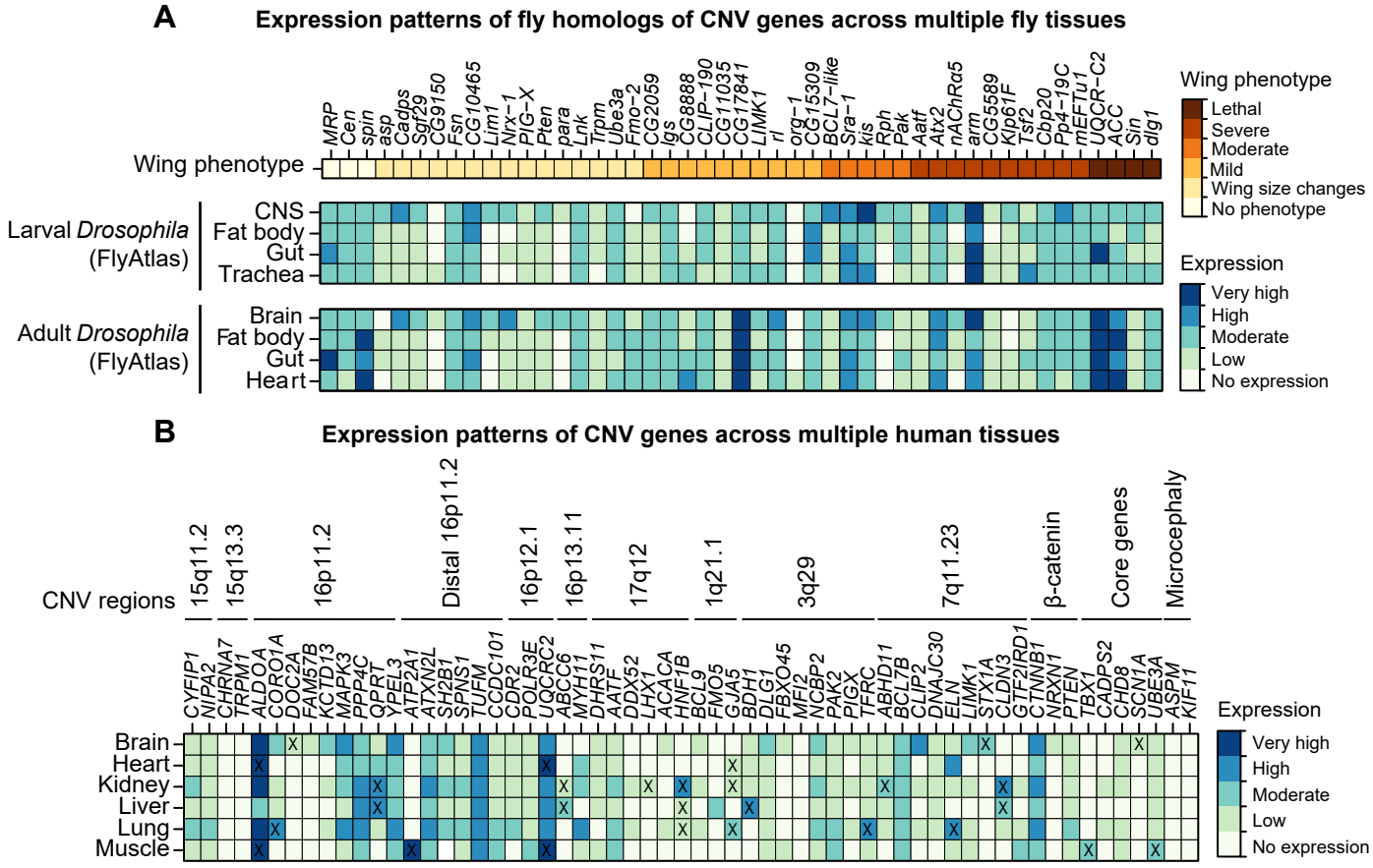
A
Expression patterns of fly homologs of CNV genes across multiple fly tissues
MRP
Cen
spin
asp
Cadps
Sgf29
CG9150
Fsn
CG10465
Lim1
Nrx−1
PIG−X
Pten
para
Lnk
Trpm
Ube3a
Fmo−2
CG2059
Igs
CG8888
CLIP−190
CG11035
CG17841
LIMK1
rl
org−1
CG15309
BCL7−like
Sra−1
kis
Rph
Pak
Aatf
Atx2
nAChRα5
arm
CG5589
Klp61F
Tsf2
Cbp20
Pp4−19C
mEFTu1
UQCR−C2
ACC
Sin
dlg1
Wing phenotype
Lethal
Severe
Moderate
Mild
Wing size changes
No phenotype
Larval Drosophila (FlyAtlas)
CNS
Fat body
Gut
Trachea
Adult Drosophila (FlyAtlas)
Brain
Fat body
Gut
Heart
Expression
Very high
High
Moderate
Low
No expression
B
Expression patterns of CNV genes across multiple human tissues
CNV regions
15q11.2
15q13.3
16p11.2
Distal 16p11.2
16p12.1
16p13.11
17q12
1q21.1
3q29
7q11.23
β-catenin
Core genes
Microcephaly
CYFIP1
NIPA2
CHRNA7
TRPM1
ALDOA
CORO1A
DOC2A
FAM57B
KCTD13
MAPK3
PPP4C
QPRT
YPEL3
ATP2A1
ATXN2L
SH2B1
SPNS1
TUFM
CCDC101
CDR2
POLR3E
UQCRC2
ABCC6
MYH11
DHRS11
AATF
DDX52
LHX1
ACACA
HNF1B
BCL9
FMO5
GJA5
BDH1
DLG1
FBXO45
MFI2
NCBP2
PAK2
PIGX
TFRC
ABHD11
BCL7B
CLIP2
DNAJC30
ELN
LIMK1
STX1A
CLDN3
GTF2IRD1
CTNNB1
NRXN1
PTEN
TBX1
CADPS2
CHD8
SCN1A
UBE3A
ASPM
KIF11
Brain
Heart
Kidney
Liver
Lung
Muscle
Expression
Very high
High
Moderate
Low
No expression

Figure 7

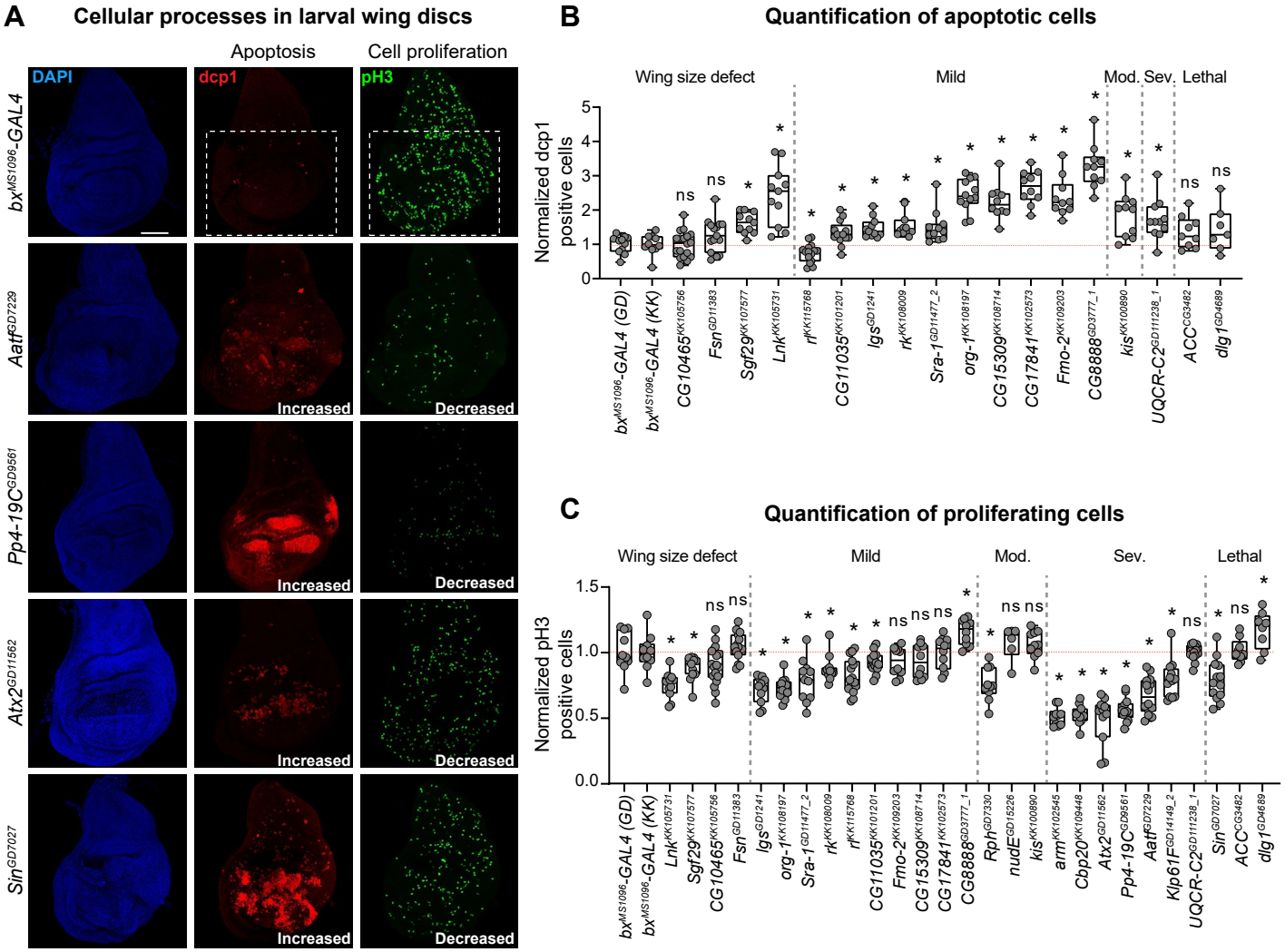
A
Cellular processes in larval wing discs
Apoptosis
Cell proliferation
DAPI
dcp1
pH3
bx^MS1096-GAL4
Aatf^GD7229
Pp4-19C^GD9561
Atx2^GD11562
Sin^GD7027
Increased
Decreased
B
Quantification of apoptotic cells
Wing size defect
Mild
Mod.
Sev.
Lethal
Normalized dcp1 positive cells
bx^MS1096-GAL4 (GD)
bx^MS1096-GAL4 (KK)
CG10465^KK105756
Fsn^GD11383
Sgf29^KK107577
Lnk^KK105731
rk^KK115768
CG11035^KK101201
Igs^GD1241
rk^KK108009
Sra-1^GD11477_2
org-1^KK108197
CG15309^KK108714
CG17841^KK102573
Fmo-2^KK109203
CG8888^GD3777_1
kis^KK100890
UQCR-C2^GD11238_1
ACC^CG3482
dlg1^GD4689
C
Quantification of proliferating cells
Wing size defect
Mild
Mod.
Sev.
Lethal
Normalized pH3 positive cells
Rph^GD7330
nudE^GD15226
arm^KK102545
Cbp20^KK109448
Atx2^GD11562
Pp4-19C^GD9561
Aatf^GD7229
Klp61F^GD14149_2
Sin^GD7027

Figure 8

Disruption of signaling pathways in larval wing discs

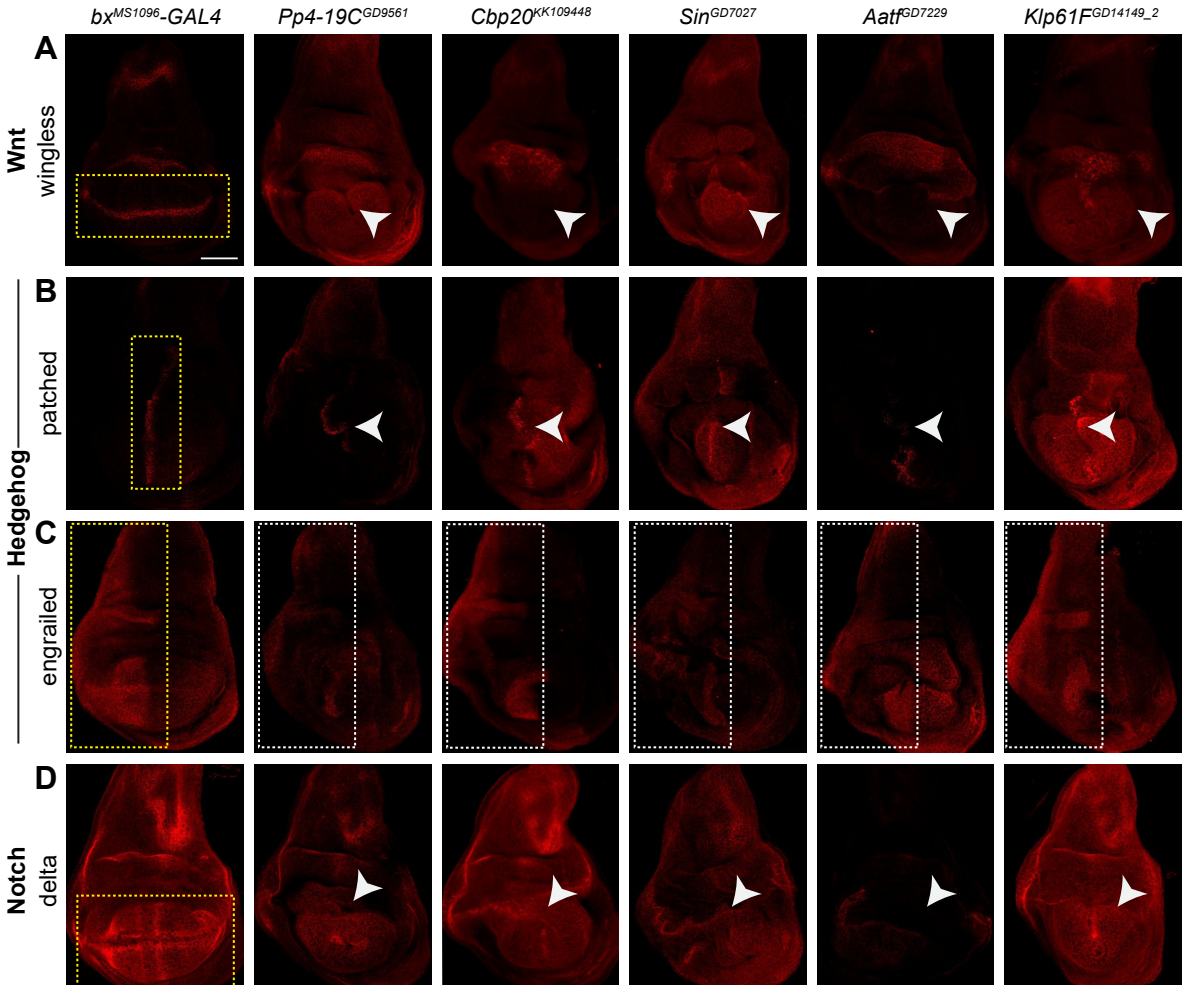

Figure 9

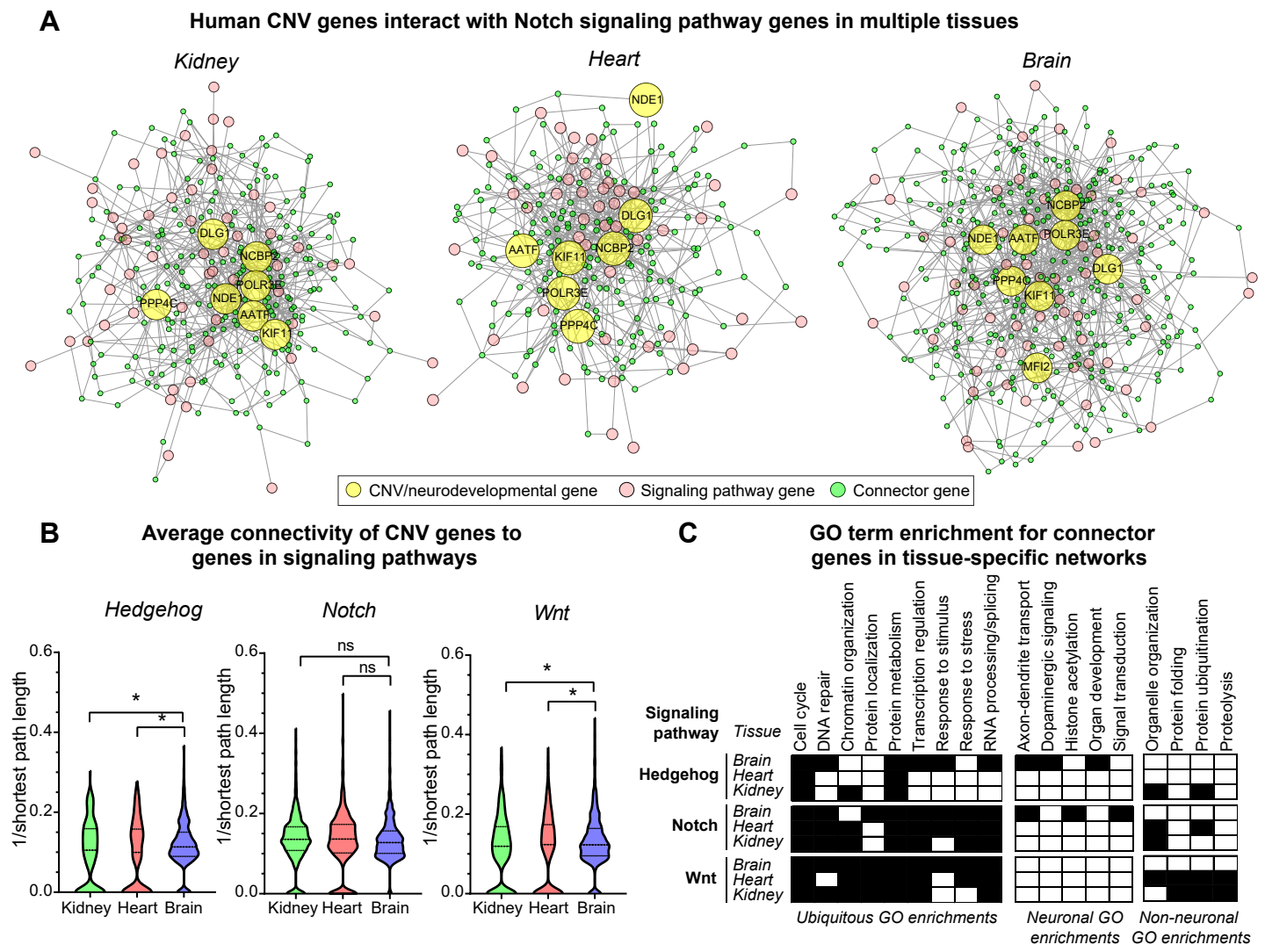
A
Human CNV genes interact with Notch signaling pathway genes in multiple tissues
Kidney
Heart
Brain
DLG1
NCBP2
POLR3E
NDE1
AATF
KIF11
PPP4C
MFI2
CNV/neurodevelopmental gene
Signaling pathway gene
Connector gene
B
Average connectivity of CNV genes to genes in signaling pathways
Hedgehog
Notch
Wnt
1/shortest path length
0.0
0.2
0.4
0.6
ns
*
Kidney
Heart
Brain
C
GO term enrichment for connector genes in tissue-specific networks
Signaling pathway
Tissue
Hedgehog
Notch
Wnt
Brain
Heart
Kidney
Cell cycle
DNA repair
Chromatin organization
Protein localization
Protein metabolism
Transcription regulation
Response to stimulus
Response to stress
RNA processing/splicing
Axon-dendrite transport
Dopaminergic signaling
Histone acetylation
Organ development
Signal transduction
Organelle organization
Protein folding
Protein ubiquitination
Proteolysis
Ubiquitous GO enrichments
Neuronal GO enrichments
Non-neuronal GO enrichments

Figure 10

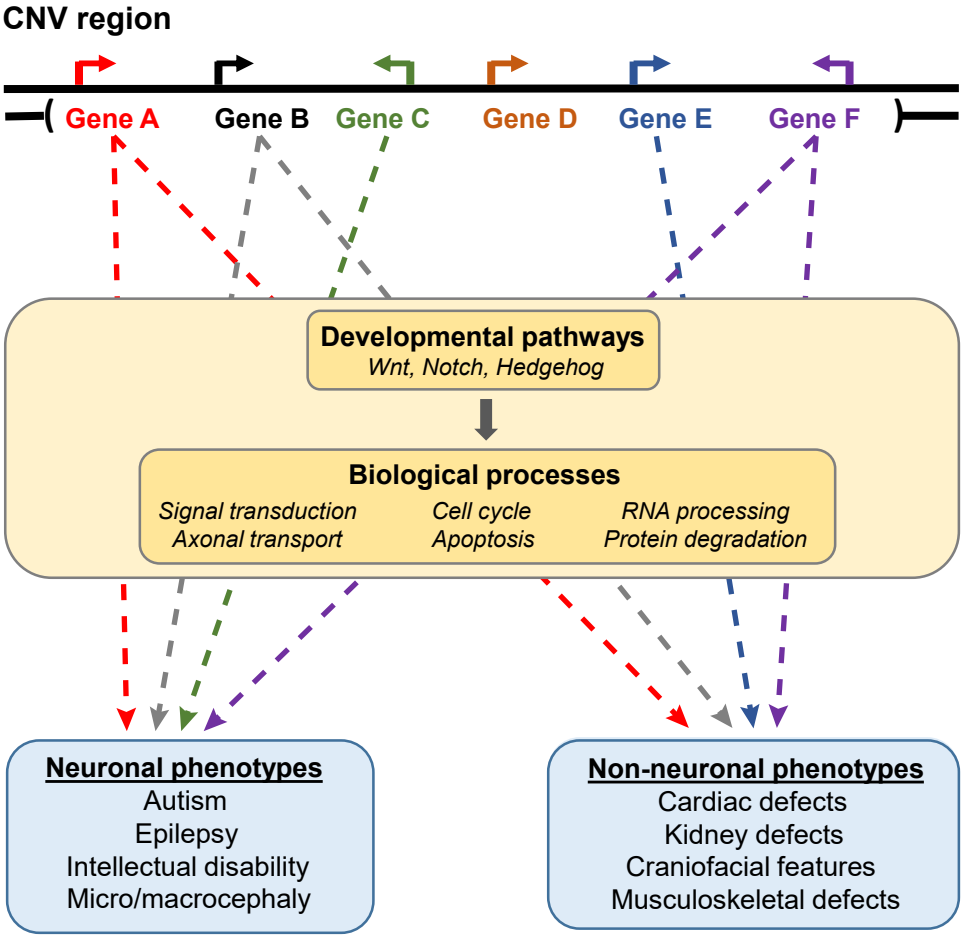
CNV region
Gene A
Gene B
Gene C
Gene D
Gene E
Gene F
Developmental pathways
Wnt, Notch, Hedgehog
Biological processes
Signal transduction
Cell cycle
RNA processing
Axonal transport
Apoptosis
Protein degradation
Neuronal phenotypes
Autism
Epilepsy
Intellectual disability
Micro/macrocephaly
Non-neuronal phenotypes
Cardiac defects
Kidney defects
Craniofacial features
Musculoskeletal defects